JAMES | Journal of Advances in Modeling Earth Systems

RESEARCH ARTICLE
10.1029/2018MS001574

PEAT-CLSM: A Specific Treatment of Peatland Hydrology in the NASA Catchment Land Surface Model

M. Bechtold[1,2], G. J. M. De Lannoy[1], R. D. Koster[3], R. H. Reichle[3], S. P. Mahanama[3,4], W. Bleuten[5], M. A. Bourgault[6], C. Brümmer[7], I. Burdun[8], A. R. Desai[9], K. Devito[10], T. Grünwald[11], M. Grygoruk[12], E. R. Humphreys[13], J. Klatt[14], J. Kurbatova[15], A. Lohila[16,17], T. M. Munir[18], M. B. Nilsson[19], J. S. Price[20], M. Röhl[21], A. Schneider[22], and B. Tiemeyer[7]

[1]Department of Earth and Environmental Sciences, KU Leuven, Heverlee, Belgium, [2]Department of Computer Science, KU Leuven, Heverlee, Belgium, [3]Global Modeling and Assimilation Office, NASA Goddard Space Flight Center, Greenbelt, MD, USA, [4]Science Systems and Applications, Inc., Lanham, MD, USA, [5]Department of Physical Geography, Utrecht University, Utrecht, The Netherlands, [6]Département des sciences de la Terre et de l'atmosphère-GEOTOP Research Center, Université du Québec à Montréal, Montréal, Québec, Canada, [7]Thünen Institute of Climate-Smart Agriculture, Braunschweig, Germany, [8]Department of Geography, Institute of Ecology and Earth Sciences, University of Tartu, Tartu, Estonia, [9]Department of Atmospheric and Oceanic Sciences, University of Wisconsin-Madison, Madison, WI, USA, [10]Department of Biological Sciences, University of Alberta, Edmonton, Alberta, Canada, [11]Institute of Hydrology and Meteorology, Technische Universität Dresden, Tharandt, Germany, [12]Faculty of Civil and Environmental Engineering, Warsaw University of Life Sciences-SGGW, Warsaw, Poland, [13]Department of Geography and Environmental Studies, Carleton University, Ottawa, Ontario, Canada, [14]Institute for Meteorology and Climatology-Atmospheric Environmental Research (IMK-IFU), Karlsruhe Institute of Technology (KIT), Garmisch-Partenkirchen, Germany, [15]A. N. Severtsov Institute of Ecology and Evolution, Russian Academy of Sciences, Moscow, Russia, [16]Climate System Research, Finnish Meteorological Institute, Helsinki, Finland, [17]Institute for Atmospheric and Earth System Research/Physics, Faculty of Science, University of Helsinki, Helsinki, Finland, [18]Department of Geography, University of Calgary, Calgary, Alberta, Canada, [19]Department of Forest Ecology and Management, Swedish University of Agricultural Sciences, Umeå, Sweden, [20]Wetlands Hydrology Lab, University of Waterloo, Waterloo, Ontario, Canada, [21]Institute of Landscape and Environment, HfWU Nürtingen, Nürtingen, Germany, [22]Institute of Botany and Landscape Ecology, University of Greifswald, Greifswald, Germany

Key Points:
- A peatland-specific land surface hydrology was added to an Earth system model and constrained by literature data, without parameter tuning
- Simulations were evaluated with a data set of groundwater table depth and evapotranspiration with unprecedented coverage in high latitudes
- The peatland model version performs significantly better in terms of hydrological variables over peatlands than the operational model

Correspondence to:
M. Bechtold,
michel.bechtold@kuleuven.be

Citation:
Bechtold, M., De Lannoy, G. J. M., Koster, R. D., Reichle, R. H., Mahanama, S. P., Bleuten, W., et al. (2019). PEAT-CLSM: A specific treatment of peatland hydrology in the NASA Catchment Land Surface Model. *Journal of Advances in Modeling Earth Systems*, *11*, 2130–2162. https://doi.org/10.1029/2018MS001574

Received 27 NOV 2018
Accepted 29 APR 2019
Accepted article online 7 MAY 2019
Published online 10 JUL 2019

Abstract Peatlands are poorly represented in global Earth system modeling frameworks. Here we add a peatland-specific land surface hydrology module (PEAT-CLSM) to the Catchment Land Surface Model (CLSM) of the NASA Goddard Earth Observing System (GEOS) framework. The amended TOPMODEL approach of the original CLSM that uses topography characteristics to model catchment processes is discarded, and a peatland-specific model concept is realized in its place. To facilitate its utilization in operational GEOS efforts, PEAT-CLSM uses the basic structure of CLSM and the same global input data. Parameters used in PEAT-CLSM are based on literature data. A suite of CLSM and PEAT-CLSM simulations for peatland areas between 40°N and 75°N is presented and evaluated against a newly compiled data set of groundwater table depth and eddy covariance observations of latent and sensible heat fluxes in natural and seminatural peatlands. CLSM's simulated groundwater tables are too deep and variable, whereas PEAT-CLSM simulates a mean groundwater table depth of −0.20 m (snow-free unfrozen period) with moderate temporal fluctuations (standard deviation of 0.10 m), in significantly better agreement with in situ observations. Relative to an operational CLSM version that simply includes peat as a soil class, the temporal correlation coefficient is increased on average by 0.16 and reaches 0.64 for bogs and 0.66 for fens when driven with global atmospheric forcing data. In PEAT-CLSM, runoff is increased on average by 38% and evapotranspiration is reduced by 19%. The evapotranspiration reduction constitutes a significant improvement relative to eddy covariance measurements.

Plain Language Summary Peatlands are wetlands in which plant matter has accumulated over thousands of years under almost permanently water-logged conditions. Alterations in these conditions as a result of global climate change can lead to the release of the huge peatland carbon pool as carbon dioxide over much shorter timescales than were required for accumulation. The additional emissions would amplify global warming. A better representation of the peatland hydrology in global Earth system models can help quantify how peatlands respond to a changing climate. In this paper, we add a peatland-specific land surface hydrology module to the land surface model used in NASA's GEOS Earth

system modeling framework. Comparisons of numerical simulations encompassing northern peatlands against field observations show that the new model version significantly improves our ability to capture the hydrological dynamics of peatlands. The new peatland representation in GEOS offers new opportunities, including the potential for merging model information and remote sensing observations in a way that improves our understanding of the overall role played by peatlands in the global water and carbon cycles.

1. Introduction

Peatlands represent 50 to 70% of global wetlands and are characterized by a surface layer of organic carbon-rich soil (peat) that can be several meters thick (Joosten & Clarke, 2002). Peat consists of partially decomposed plant matter that accumulated in place over thousands of years due to reduced aerobic decomposition under permanently shallow groundwater tables (Clymo et al., 1998). The two major categories of peatlands are bogs, which are rain-fed (ombrotrophic), and fens, which also receive lateral water input from groundwater and—sometimes—surface water (e.g., rivers and lakes). The resulting characteristic hydrologic and nutrient conditions have led to unique habitats for various highly adapted ecosystems. These ecosystems in turn provide the substrate for new peat layers, thereby strongly influencing the habitat via various stabilizing internal feedbacks (Belyea & Baird, 2006; Waddington et al., 2015).

Through peatland formation, an enormous carbon stock of 400 to 600 Gt, or approximately one third of the global terrestrial soil carbon, accumulated during the Holocene over only 3 to 4% of the land surface (Frolking et al., 2011; Loisel et al., 2014). About 80 to 90% of this stock is located in the temperate, boreal, and subarctic zones of the Northern Hemisphere. In some regions, peatlands are the dominant land cover, in particular south of the continuous permafrost boundary in Canada and the Western Siberian Lowlands (Xu et al., 2018). Over timescales of a hundred years and more, natural peatlands have a cooling effect on the climate since the negative global warming potential of the continuous net carbon dioxide (CO_2) sink exceeds the positive global warming potential of the methane (CH_4) emissions from peatlands, given the short atmospheric lifetime of CH_4 (~10 years; Frolking et al., 2011; Frolking & Roulet, 2007). Apart from the obvious reversal of the net carbon flux after the drainage of a peatland for agricultural use (Tubiello et al., 2016), the greenhouse gas balance could also change if peatland ecosystems and their associated hydrologic conditions were to be destabilized by more subtle alterations, for example, due to climate change or N deposition (Limpens et al., 2008). Substantial parts of the global peatland carbon pool could potentially be released to the atmosphere over a much shorter time period than that needed to accumulate the carbon (Dorrepaal et al., 2009; Limpens et al., 2008).

The role played by peatlands in past and future climate continues to be an important subject of research (Limpens et al., 2008). Various modeling frameworks have been developed or adapted to include peatland processes. While a few focus on peatland processes at millennial timescales (e.g., Frolking et al., 2010; Morris et al., 2012), the majority are based upon field observations of water, energy, and carbon cycles and are constructed for application at shorter timescales and at local to regional spatial scales. Many of these peatland models use observed groundwater table depth as an input to simulate the effects of moisture, temperature, and vegetation properties on carbon dynamics (e.g., Frolking et al., 2002; Metzger et al., 2015; St-Hilaire et al., 2010). Other models are hydrologically more sophisticated and include a modeling of dynamic groundwater table depth (Borren & Bleuten, 2006; e.g., Dimitrov et al., 2011; Gong et al., 2012; Granberg et al., 1999; Grant et al., 2012; Sonnentag et al., 2008; Wu & Blodau, 2013; Zhang et al., 2002). These studies have demonstrated the importance of lateral water fluxes and detailed vegetation descriptions for accurate water cycle simulations.

The above modeling efforts used detailed site-specific input information (e.g., on soil hydraulic properties and vegetation composition) and parameters that were tuned to fit observations at individual sites. This approach is adequate for understanding the local complex interactions between soil and plant processes that determine peatland behavior (Grant et al., 2012). However, such an approach would not be suitable for global land surface modeling schemes, given computational constraints and limited access to high-resolution input and tuning data across the globe. As a consequence, peatlands are rather poorly represented in global Earth system models that simulate the water, energy, and carbon cycles at daily or subdaily resolution. Only 3 out of 10 models participating in a recent intercomparison of global wetland and wetland CH_4 emission models included a peatland-specific hydrology module (Melton et al., 2013). In general, peatland

feedbacks on climate are not yet properly accounted for in predictions of future climate change (Intergovernmental Panel on Climate Change, 2014).

Attempts to include peatland hydrology in Earth system models include a representation in the Canadian Land Surface Scheme (CLASS), a 1-D soil-vegetation-atmosphere transfer model. CLASS was the first globally applicable framework with a specific parameterization for peat soils. Using Clapp and Hornberger (1978), Letts et al. (2000) parameterized the typical decline of saturated hydraulic conductivity and coarser pores with depth over three soil layers of different decomposition states, based on literature data of fibric, hemic, and sapric organic matter (representing fresh, moderately decomposed and highly decomposed organic matter, respectively). Recently, the soil layering has been further modified in CLASS by adding layers including a 10-cm moss layer at the top, so that part of the peatland vegetation is modeled like soil in order to buffer realistically the exchange of energy and water at the soil surface (Wu et al., 2016). In addition to imposing a low saturated hydraulic conductivity for the sapric peat at the bottom of the profile, a drainage reduction factor ranging from 0 to 0.3 (Letts et al., 2000) is imposed to limit the one-dimensional gravitational drainage through the bottom and keep simulated groundwater tables shallow. In contrast to CLASS, the peatland module of the Lund-Potsdam-Jena (LPJ) model includes lateral discharge through the subsurface (Wania et al., 2009).

Lawrence and Slater (2008) incorporated thermal and hydraulic properties of organic soil into the Community Land Model (CLM) and investigated, using coupled land-atmosphere simulations, the resulting effects on climate. They did not, however, simulate a dynamic groundwater table. Shi et al. (2015) recently modified CLM to represent the hydrology (including the groundwater table) of an ombrotrophic raised-dome bog in Northern Minnesota (S1-Bog). In contrast to CLASS and LPJ, they took into account the effect of microtopography on groundwater table fluctuations, and this led to more realistic fluctuations at shallow groundwater tables. Similarly, Bohn et al. (2013) implemented a microtopography treatment into the Variable Infiltration Capacity (VIC) model. Both microtopography implementations, however, utilized parameter tuning for certain areas, and the general applicability of the models was not demonstrated by evaluating simulations against hydrological field data from independent areas.

Recently, a peatland version of the Organising Carbon and Hydrology In Dynamic Ecosystems (ORCHIDEE) model was introduced (Qiu et al., 2018). While the CLASS, LPJ, and CLM peatland concepts assume a bog scenario by neglecting lateral surface water or groundwater input, the peatland version of Organising Carbon and Hydrology In Dynamic Ecosystems converts all surface runoff from the nonpeatland fraction of a grid cell into an additional water input into the peatland fraction of that cell. In addition, subsurface drainage is set to zero. A comparison of simulation results with field observations from northern peatland sites showed low temporal correlation coefficients ($R < 0.32$), reflecting the difficulty of integrating lateral water inputs into peatland models.

As part of a general revision of the land surface scheme used in the European Centre for Medium-Range Weather Forecasts' Integrated Forecasting System, Balsamo et al. (2009) introduced an *organic* soil texture class. Similarly, De Lannoy et al. (2014) added a peat soil class to the Catchment Land Surface Model (CLSM; Koster et al., 2000), the land model component of the NASA Goddard Earth Observing System (GEOS) modeling framework, and one of the few such global land models to simulate groundwater tables. The effect of the parameter update was evaluated for soil moisture in mineral soils but not for peatlands due to a lack of sufficient peat soil moisture data. With a focus on permafrost dynamics, Chadburn et al. (2015) added a representation of organic soils to JULES, the land surface scheme of the UK Earth System Model. Their model evaluation was restricted to active layer thickness and soil temperature.

In this paper we aim to advance the treatment of peatland hydrology in global Earth system modeling frameworks. More specifically, we present the implementation of a new treatment of peatland hydrology into the GEOS CLSM. The GEOS framework is used for several operational global data assimilation and forecast products (https://gmao.gsfc.nasa.gov/products/); it underlies, for example, the Modern-Era Retrospective analysis for Research and Applications version 2 climate reanalysis (MERRA-2; Gelaro et al., 2017) and the Soil Moisture Active Passive (SMAP) mission Level-4 Soil Moisture (SM_L4) data assimilation product (Reichle et al., 2017). We aim to amend the GEOS CLSM for peatlands with an emphasis on a plausible global application (i.e., in a computationally efficient way without the need for local tuning) to reduce obstacles to its eventual use in GEOS operations.

The structure of the paper is as follows. In section 2, we introduce the general modeling concept of CLSM and describe the modifications built into our peatland module for CLSM, hereafter referred to as PEAT-CLSM. In section 3, we describe our experimental design and evaluation approach. A unique aspect of this paper is the comparison of simulation results to an unprecedentedly large data set of groundwater table and evapotranspiration observations from natural to seminatural northern peatlands. Section 4 presents our results, and section 5 concludes with an overview of the benefits of PEAT-CLSM, along with a list of remaining research issues.

2. Model Description

2.1. The Catchment Land Surface Model (CLSM)

CLSM is a state-of-the-art land surface water and energy budget model designed for the use in global Earth system models (Ducharne et al., 2000; Koster et al., 2000). Below we describe some key features of CLSM, for which the basic spatial computational unit is the irregularly shaped hydrological *catchment*, though the model can also be run on grid cells. This summary focuses on aspects of CLSM relevant to the peatland-specific modifications presented afterward. For further reading on CLSM and its components, see Ducharne et al. (2000), Koster et al. (2000), Koster and Suarez (1992), De Lannoy et al. (2014), and Tao et al. (2017).

2.1.1. Groundwater Table Depth, Soil Moisture, and Dynamical Surface Partitioning

CLSM simulates a dynamic groundwater table with a spatial distribution related to catchment topography characteristics via the TOPMODEL formulation (Beven & Kirkby, 1979):

$$z_{WT} = \bar{z}_{WT} + \frac{1}{\upsilon}\left(\ln\frac{A}{\tan\beta} - \bar{x}\right) \tag{1}$$

where z_{WT} is groundwater table depth (m; negative below the surface), $\ln(A/\tan\beta)$ is the *compound topographic index* at a point within the catchment, A is the upstream area that contributes flow through a unit contour positioned at the point, β is the terrain slope at the point, $\bar{z}_{WT}$ is the catchment mean groundwater table depth, $\bar{x}$ is the mean catchment value of $\ln(A/\tan\beta)$, and υ is a parameter describing the decrease of saturated hydraulic conductivity with depth. Each catchment is characterized by its topographic index distribution, which in effect is used to diagnose the spatial variability of soil moisture within the catchment from the catchment element's three bulk water prognostic variables. Figure 1a illustrates this for one of these prognostic variables, that is, the *catchment deficit* (mm), which represents the average amount of water, per unit area, that would have to be added to bring all of the soil throughout the catchment to saturation, assuming that the unsaturated zone is in equilibrium. The other two soil water-related prognostic variables in CLSM are the *surface layer excess* and the *root zone excess*, which capture, respectively, the degree to which water (mm) in the near-surface soil (0 to −5 cm) and the root zone soil (0 to −100 cm) exceeds (or is in deficit of) amounts corresponding to equilibrium conditions in response to evapotranspiration and precipitation processes.

With this framework, three dynamic areal fractions (F) are diagnosed at each time step, each representing a distinct hydrological regime: the wilting (F_{wilt}), the unsaturated-but-transpiring (F_{tra}), and the saturated (F_{sat}) regimes, with $F_{wilt} + F_{tra} + F_{sat} = 1$. To generate these areas, an equilibrium moisture profile is assumed above a given groundwater table depth, and the integral of that profile from the surface to a depth of 1 m is taken to be the (local) equilibrium root zone moisture. Because CLSM effectively follows a distribution of groundwater table depths as represented by the TOPMODEL framework, this translates to a corresponding probability density function of equilibrium root zone soil moisture contents. The root zone excess variable shifts this distribution to the right or left: this shifted probability density function is then used to partition the catchment into the three hydrological regimes. In practice, for a given catchment, the effects of this treatment are captured with empirical functions based on extensive precalculations using that catchment's distribution of topographic indices (Ducharne et al., 2000). The diagnosed areal fractions are fundamental to CLSM, as different evapotranspiration and runoff physics are applied in each.

The vertical water flux between the surface layer and the root zone is controlled by a timescale, τ, computed with

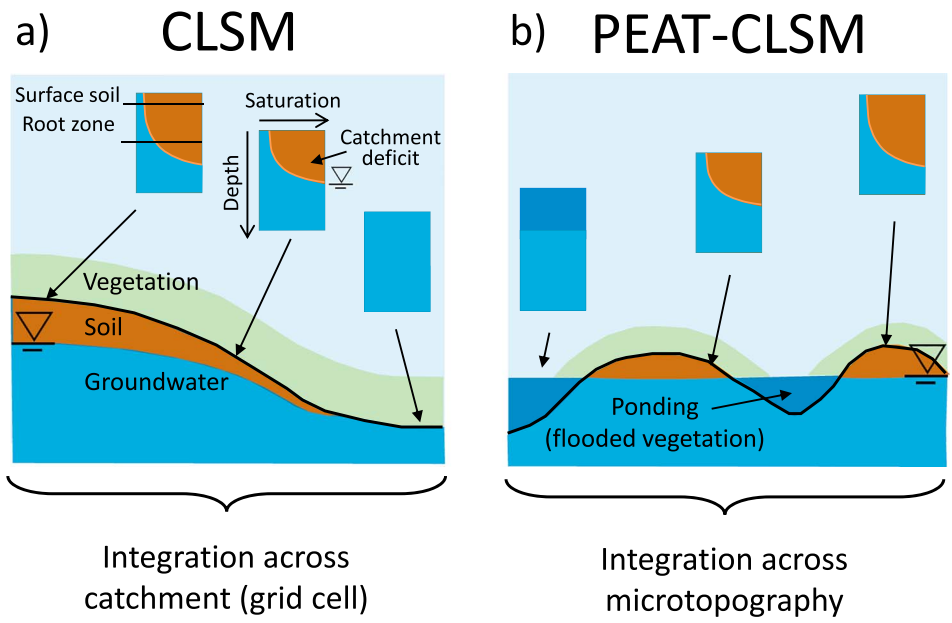

Figure 1. Schematic illustration of the two different spatial scales across which (a) CLSM and (b) PEAT-CLSM integrate groundwater table depth and soil moisture variability, shown here for the (light brown) *catchment deficit* variable under hydrostatic equilibrium conditions.

$$\tau = \frac{a_r}{(\theta_{rz} + b_r M_{se})^3} \tag{2}$$

Here a_r and b_r are fitted parameters, θ_{rz} is the diagnosed catchment mean root zone moisture content (m^3/m^3), and M_{se} is the surface layer excess (m). The water transfer between the surface layer and the root zone, ΔM_{se} (m), during a time period Δt is

$$\Delta M_{se} = -M_{se}\frac{\Delta t}{\tau} \tag{3}$$

The empirical equation for the timescale τ (equation (2)) is fitted to results from high-resolution (1-cm) simulations of the vertical one-dimensional Richards equation that were conducted offline prior to running any CLSM simulations. These high-resolution offline simulations use a comprehensive set of values for the CLSM's water prognostic variables (Ducharne et al., 2000) appropriately downscaled to 1-cm resolution, with a soil-specific Campbell parameterization (Campbell, 1974; De Lannoy et al., 2014) applied within each 1-cm element:

$$\frac{h}{h_s} = \left(\frac{\theta}{\theta_s}\right)^{-b} \tag{4}$$

$$K = K_s\left(\frac{\theta}{\theta_s}\right)^{2b+3} \tag{5}$$

where θ_s (m^3/m^3) is the volumetric soil moisture content at saturation, h is pressure head (cm H_2O), h_s (cm H_2O) is the air entry pressure, b is an empirical shape parameter, K_s (m/s) is the saturated hydraulic conductivity, and K (m/s) is the unsaturated hydraulic conductivity. The corresponding approach for the water transfer between catchment deficit and root zone excess, ΔM_{rz}, is similar though more strongly tied to topographical variations (see Ducharne et al., 2000).

2.1.2. Soil Temperature and Snow Modeling

CLSM uses a six-layer heat diffusion model to simulate subsurface soil temperatures in terms of soil heat contents (Koster et al., 2000). Furthermore, a three-layer snow model describes the state of the snowpack in terms of snow water equivalent, snow depth, and snow heat content (Stieglitz et al., 2001). The

modeled snow layer buffers the heat and water exchange between atmosphere and land. A dynamic ice fraction is simulated for each of the six soil layers of the heat diffusion model. A detailed description of the freeze-thaw model is presented in Tao et al. (2017). The revised permafrost model in that paper was not utilized here.

2.1.3. Runoff

The total runoff is the sum of a subsurface (base flow) component and a surface runoff (overland flow) component. Base flow is directly related to $\overline{z}_{WT}$ using TOPMODEL equations (Koster et al., 2000). The simulated ice fraction (section 2.1.2) is used to linearly reduce the base flow rate. Overland flow includes a Dunne (saturation excess) component and a Hortonian (infiltration excess) runoff component. In the *saturated fraction* regime, all throughfall (precipitation minus interception) and snowmelt water runs off the surface, effectively as Dunne runoff; none of this water infiltrates. Elsewhere, infiltration excess occurs when the remaining throughfall and snowmelt water exceeds the air-filled porosity of the surface layer of F_{tra} and F_{wilt}. Ponding on top of the ground surface and *run-on* processes (i.e., routing of water over the land surface for infiltration at a different place) are not simulated in CLSM. All runoff (base flow, saturation excess, and infiltration excess) is immediately removed from the system.

2.1.4. Surface Energy Balance

The surface energy balance is computed separately for the three hydrological regimes (F_{sat}, F_{tra}, and F_{wilt}) of a catchment. CLSM computes each regime's canopy conductance from meteorological input data, prescribed vegetation phenology (namely, leaf area index, or LAI, and greenness fraction), and regime-specific temperature and moisture prognostic variables; these conductances are then used in regime-specific energy balance calculations. The energy balance calculations are largely based on those in the Simple Biosphere Model (Sellers et al., 1986), which were simplified to be consistent with the Penman-Monteith formulation (Koster & Suarez, 1992). Given the different moisture states of the three regimes, both energy-limited and water-limited evapotranspiration fluxes are captured. In general, modeled evapotranspiration rates over F_{sat} are higher than evapotranspiration rates over F_{tra}, which in turn are higher than those over F_{wilt}.

2.2. PEAT-CLSM

PEAT-CLSM is a peatland-specific land surface hydrology module for CLSM. It is intended for the application over all grid cells (or catchments) that are classified as peat according to the recent revision of the soil map of CLSM (De Lannoy et al., 2014). A spatially complete land surface simulation, encompassing both peat and mineral soils (not applied here), could be achieved by using the original Catchment model approach (section 2.1) for the grid cells (or catchments) with mineral soils after deriving new catchment topographic index statistics that exclude peatlands. The details of such an approach are left for future work.

CLSM does not take into account any water management. Similarly, we treat all peatlands as being natural; that is, drainage practices to establish agriculture, forestry, or mining are not accounted for in PEAT-CLSM.

2.2.1. Microtopography and Surface Water Ponding

The TOPMODEL approach underlying equation (1) is not suitable for peatlands for two reasons. First, a large fraction of global peatlands is hydraulically decoupled from the large-scale catchment groundwater hydrology. This is the case for bogs and also to some extent for fens that are, for example, (partly) underlain by confining layers and/or receive lateral water input from surrounding bogs (rather than from the groundwater of the larger-scale watershed). Second, on a macrotopographic scale of thousands of meters, most peatlands (apart from a few peatland types, e.g., blanket bogs, and the margin areas of bogs) are virtually flat. Over such flat terrain, the derivation of the topographic index distribution from global elevation data is likely very inaccurate given the difficulties in determining slope, flow direction, and accumulation area (Kienzle, 2004).

In PEAT-CLSM, we therefore discard the use of the TOPMODEL concept for computing macrotopographic effects on the distribution of groundwater table depth and base flow. Instead, we compute the latter as function of a microtopographic distribution (Figure 1b), a characteristic feature of peatlands in general (Rydin et al., 2006) that is critical for the description of the water storage. Note that our rejection of the TOPMODEL formulation in PEAT-CLSM for macrotopographical effects in peat grid cells implies that we treat all peatlands as being fully decoupled from surrounding catchment hydrology and as being only fed by direct precipitation over the peat grid cell. We emphasize that the current PEAT-CLSM concept does not address specific features of fen-like systems that cover, for example, vast areas of peatlands in the

Table 1
Overview of Studies With Quantitative Information on Microtopography

Reference	Peatland type and location	Microtopography information (m)		
		Maximum to minimum elevation	Mean elevation difference between hummock and hollow	Standard deviation of elevations
Dettmann and Bechtold (2016a)	Bog (Schechenfilz, Germany)	0.3	0.2	0.06 to 0.09
Nungesser (2003)	Bog (Howland, USA)	0.6	0.29 +/- 0.09	n/a
Kettridge et al. (2008) and Nungesser (2003)	Bog (Caribou, USA)	0.6	0.43 +/- 0.12	n/a
Johnson et al. (1990)	Bog (Akhult, Sweden)	n/a	0.2 to 0.3	n/a
van der Schaaf (1999)	various bogs (Irland)	n/a	0.4	n/a
Lafleur et al. (2005) and Malhotra et al. (2016)	Bog (Mer Bleue, Canada)	n/a	0.25	0.07
Shi et al. (2015)	Bog (S1-Bog, USA)	n/a	0.3	n/a
Frei et al. (2010)	Fen (Lehstenbach, Germany)	0.6	0.2 to 0.4	n/a
Price (1997)	Bog-Fen complex (Lac Saint-Jean, Canada)	n/a	0.3	n/a
Rochefort et al. (1990)	Fen (Experimental Lakes Area, Canada)	n/a	0.28	n/a

Boreal Plains (Western Canada) where additional water inputs from minerogenic groundwater and/or adjacent peatlands are required due to insufficient annual precipitation. The groundwater influence in fens is very difficult to parameterize and could perhaps be addressed with a blended modeling that combines PEAT-CLSM with information about how peatlands are embedded in the landscape.

Table 1 gives an overview of peatland studies that provide quantitative characterizations of microtopography. The two most detailed studies showed that the measured elevations can be approximated by a normal distribution (Dettmann & Bechtold, 2016a; Malhotra et al., 2016) with standard deviations ranging from 0.06 to 0.09 m. Other works give information on the mean and maximum elevation difference between hummocks and hollows, the two major microtopographic elements in peatlands. Reported mean elevation differences vary between 0.2 and 0.43 m; reported maximum differences can reach up to 0.6 m. Table 1 lacks data concerning hummock and hollow microtopography in the Western Siberian Lowlands, which is one of the largest peatland areas on Earth. Nevertheless, Terentieva et al. (2016) and Eppinga et al. (2008) provide estimates of elevation differences of 0.4–0.7 m between ridges and hollows characteristic of West Siberian boreal bog-fen complexes. However, these landscape elements occur over a spatial scale of 10–100 m, while the spatial scale of a typical hummock-hollow microtopography is only a few meters. In PEAT-CLSM, both features will be simulated by the same concept.

Microtopography modulates groundwater table dynamics (Ivanov, 1981) by (i) controlling the ponding of water in the hollows and (ii) determining the spatially variable thickness of the unsaturated zone above the groundwater table (Dettmann & Bechtold, 2016b). Data collected in a dense groundwater table monitoring network in the Mer Bleue bog (Table 1; Malhotra et al., 2016) showed that the spatial variability of groundwater table depth there results almost solely from microtopographic elevation variability. Hydraulic gradients between hummocks and hollows in this bog were negligible and only of short duration.

We utilize the basic CLSM framework to numerically capture the two major microtopographic effects of ponding and of the variable thickness of the unsaturated zone in a straightforward way. Figure 1b illustrates how the spatial integration scale for groundwater table depth and soil moisture variables changes from the catchment scale in CLSM to the scale of the microtopography in PEAT-CLSM. By replacing the distribution for $\ln(A/\tan\beta)$ in equation (1) with a normal distribution of microtopographic elevations and by setting $\upsilon = 1$, the subsurface modeling concept of CLSM (section 2.1.1) can represent the spatial variability of groundwater table depths with a normal distribution that solely depends on elevation variability. In contrast to CLSM, PEAT-CLSM allows the ponding of water above the saturated soil profile of F_{sat}. The surface water level of the ponded water column is assumed always to be in equilibrium with the groundwater table in the soil profile of the unsubmerged area (F_{tra} and F_{wilt}).

To date, a globally harmonized peatland map differentiating between peatland types, for example, bogs and fens, does not exist (Xu et al., 2018), making this differentiation impossible in global models. This lack of

spatial differentiation forces us to impose a single value worldwide for the standard deviation of the microtopographic elevation distribution in peatlands. Table 1 shows two reported standard deviations, but their corresponding mean elevation differences between hummocks and hollows seem to be at the low end of the reported range from other studies. Aside from the hummock-hollow microtopography, larger-scale (but still subgrid scale for global land surface models) periodic features of peatland topography like ridges and hollows in the Western Siberian Lowlands (Terentieva et al., 2016) may further increase the overall standard deviation of elevations in some areas. In the end, we subjectively combined the heterogeneous information about elevation variability and assumed a standard deviation of 0.11 m for PEAT-CLSM. This value is slightly higher than the values reported in two of the studies of Table 1.

2.2.2. Runoff and Maximum Infiltration Rate Through Macropores

The surface layers of peat are formed by weakly decomposed and little compacted plant residues. As a consequence, there is a high fraction of connected large pores (macropores) in these layers, which allow for high flow rates when saturated. The saturated hydraulic conductivity of peat, however, exponentially decreases with depth by orders of magnitude over only a few tens of centimeters (Hogan et al., 2006; Letts et al., 2000; Morris et al., 2015; Romanov, 1968) due to the increasing degree of decomposition and shift from large to small pores with depth (Baird, 1997; Dimitrov et al., 2010; Rezanezhad et al., 2012). This characteristic vertical peat structure controls the water storage dynamics of peatlands, which in turn control the biological functions that create that structure.

The saturated-unsaturated hydraulic dynamics associated with the macropore domain and the finer-pored peat matrix is bimodal in nature and is poorly represented in unimodal approaches such as that used in CLSM (equations (4) and (5); Dettmann et al., 2014; Dimitrov et al., 2010; Weber et al., 2017). In PEAT-CLSM, we therefore define two different *saturated* hydraulic conductivities. The first, $K_{s,\mathrm{macro}}$ (m/s), represents the conductivity at full saturation conditions and relates to fluxes in the macropore domain. $K_{s,\mathrm{macro}}$ is used to control lateral subsurface runoff and the downward water flux between a fully saturated surface layer and the root zone (see also discussion later in this section). The second, K_s, represents the conductivity at matrix saturation and is applied in the vertical flow module of section 2.1.1 to obtain the timescale parameters for vertical moisture transfer under unsaturated conditions. The hydraulic properties of the peat matrix are presented for PEAT-CLSM in section 2.2.3.

The peatland situation with a layer (the *acrotelm*) of very high values of $K_{s,\mathrm{macro}}$ (10^{-5} to 10^{-3} m/s) that overlies a layer (the *catotelm*) of very low hydraulic conductivities (~10^{-7} m/s) can be considered in terms of an aquifer-aquitard analogue (Ingram, 1978; van der Schaaf, 1999). The extreme $K_{s,\mathrm{macro}}$ profile has several implications for runoff dynamics. Given the high near-surface $K_{s,\mathrm{macro}}$, Hortonian (infiltration excess) runoff does not occur, causing total runoff from peatlands to be strongly reduced during deep groundwater table stages during which there is also little base flow through the catotelm (Fitzgerald et al., 2003; Holden & Burt, 2003; Weiss et al., 2006). Runoff rates increase exponentially with rising groundwater tables in the acrotelm. Since water begins to pond in depressions of the microrelief when groundwater tables rise, base flow and overland flow occur simultaneously, a mechanism known as *semisurficial runoff* (Romanov, 1968). Due to the mostly very gentle slopes in peatlands, the flow does not become turbulent, and Darcy's law is still adequate for flow calculations. This, of course, does not hold for peatlands with steeper slopes, for example, blanket bogs with specific runoff mechanisms operating during high groundwater table stages (Holden & Burt, 2003). Such bogs represent a minor portion of global peatlands and are not considered here.

The runoff formulations in CLSM were fundamentally revised for PEAT-CLSM to mimic the above runoff behavior. Based on detailed field observations, K. E. Ivanov (his work given in Romanov, 1968) suggested that a single power function relating total runoff to $\overline{z}_{\mathrm{WT}}$ is an adequate approximation for the continuously increasing total runoff seen with rising groundwater tables. We use his work in combination with theoretical and experimental field work of van der Schaaf (1999) to constrain a function originally suggested by Ivanov and given in Romanov (1968) to describe the decrease of $K_{s,\mathrm{macro}}$ for the acrotelm layer:

$$K_{s,\mathrm{macro}}(z) = \frac{K_{s,\mathrm{macro},z=0}}{(1-100z)^m} \tag{6}$$

where z (m) is the vertical position with respect to ground surface level (mean surface elevation averaged over hummock and hollow microtopography), $K_{s,\mathrm{macro},z\,=\,0}$ (m/s) is $K_{s,\mathrm{macro}}$ at the mean surface elevation

($z = 0$ m), and m is an empirical parameter describing the rate of decrease of $K_{s,\mathrm{macro}}$ with depth. Note that $K_{s,\mathrm{macro}}$ is not a soil property but rather a property of the whole system, determining, for example, the contribution of overland flow in hollows.

The lateral flow rate in the acrotelm depends on the transmissivity T_a (m^2/s), which is defined as the integral of $K_{s,\mathrm{macro}}(z)$ from the lower boundary of the acrotelm z_{ac} to $\bar{z}_{\mathrm{WT}}$ (the water table is assumed to be within the acrotelm):

$$T_a(\bar{z}_{\mathrm{WT}}) = \int_{z_{ac}}^{\bar{z}_{\mathrm{WT}}} K_{s,\mathrm{macro}}(z)dz \tag{7}$$

At the catotelm-acrotelm boundary, $K_{s,\mathrm{macro}}$ is typically already very low; its contribution to T_a can be assumed minor. As the exact thickness of the acrotelm (ranging between 0.3 and 0.7 m; Ivanov, 1981) is unknown at large scales, we assume (following van der Schaaf, 1999) that $z_{ac} \sim \infty$; that is, equation (7) is applied down to an infinite depth, knowing that contributions to the integral at the deeper depths are negligible. Equation (7) can then be written as

$$T_a(\bar{z}_{\mathrm{WT}}) = \frac{K_{s,\mathrm{macro},z=0}(1-100\bar{z}_{\mathrm{WT}})^{1-m}}{100(m-1)} \text{ for } m>1 \tag{8}$$

Assuming that horizontal hydraulic gradients in peatlands vary little over time (closely following the terrain surface slope; e.g., Ivanov, 1981, van der Schaaf, 1999) and following Darcy's law, total (lateral) runoff, Q (m/s) is proportional to T_a (van der Schaaf, 1999):

$$Q(\bar{z}_{\mathrm{WT}}) = cT_a(\bar{z}_{\mathrm{WT}}) \tag{9}$$

where c (m^{-1}) is the average hydraulic gradient divided by the average length (in flow direction) of the acrotelm layer.

In summary, the function $Q(\bar{z}_{\mathrm{WT}})$ is defined by three parameters: $K_{s,\mathrm{macro},z=0}$, m and c. Typical values of $K_{s,\mathrm{macro},z=0}$ and m are given in Romanov (1968). Furthermore, van der Schaaf (1999) found that $\log_{10}(K_{s,\mathrm{macro},z=0})$ and m are positively linearly correlated within individual peatlands and across peatlands, meaning that $K_{s,\mathrm{macro}}$ declines faster with depth for an acrotelm with a high $K_{s,\mathrm{macro},z=0}$ than it does for one with a small $K_{s,\mathrm{macro},z=0}$. For PEAT-CLSM, we prescribe the representative pair of values $K_{s,\mathrm{macro},z=0} = 10$ m/s and $m = 3$. Note that $K_{s,\mathrm{macro},z=0}$ defines the conductivity for a situation with a groundwater table at $z = 0$ m in which *semisurficial* runoff occurs. $K_{s,\mathrm{macro},z=0}$ is therefore orders of magnitude higher than $K_{s,\mathrm{macro}}$ of the acrotelm layer. Because typical values of c could not be extracted from these earlier studies, we derived a representative value from the few existing relevant observations. Figure 2 shows data from one study in which measured Q varies with $\bar{z}_{\mathrm{WT}}$ in a natural bog and a natural fen site (Weiss et al., 2006). We used these data to constrain the value of c to 1.5×10^{-7} m^{-1}; this value produces an average runoff function that describes data at both sites fairly well.

In CLSM, Hortonian runoff is generated when throughfall or snowmelt exceeds the available air-filled pore space in the surface layer. Subsequent drainage of surface layer moisture to the soil below (controlling, in effect, this air-filled pore space) is based on high-resolution precomputations of the Richards equation along with a Campbell parameterization of the hydraulic characteristics of soils with a uniform pore size distribution (see section 2.1.1). Given the very high values of $K_{s,\mathrm{macro}}$ in the acrotelm layer, we disabled the Hortonian runoff mechanism in PEAT-CLSM, allowing all water to infiltrate. Any infiltration excess predicted by the vertical flow module based on the peat matrix properties defined in 2.2.3 is allowed to infiltrate into the root zone layer via macropores. This means that the ponding of water at the soil surface described in section 2.2.1 can only occur above a saturated soil profile, that is, above F_{sat}. Note that in PEAT-CLSM the grid cell never saturates entirely (in practice) due to the highly exponential runoff function (Figure 2).

As in CLSM, we used the modeled ice fraction to linearly reduce Q in PEAT-CLSM. In PEAT-CLSM, the ice fraction applied is that in the top layer (0 to −10 cm) of the heat diffusion model instead of that in the whole soil profile, as it is the top layer that controls most of the runoff (Figure 2). A computationally more

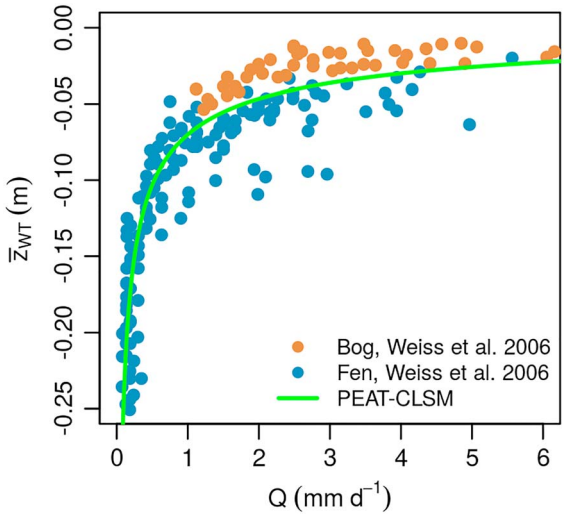

Figure 2. Relationship between total runoff Q (mm/day) and spatial mean groundwater table depth $\overline{z}_{WT}$ (m). Field observations were extracted from Weiss et al. (2006) and include data from (blue) a fen and (light brown) a bog site. The runoff function of PEAT-CLSM is shown as a green line.

intensive approach that takes into account the ice fraction of each soil layer when integrating equation (7) was not realized. Furthermore, rain water falling on an entirely frozen top soil does not generate surface runoff; that is, water is assumed to infiltrate through macropores and to fill the hollows of the microtopography.

2.2.3. Hydraulic Properties of Peat Matrix

For CLSM, vertically homogenized soil texture data for the 0 to −100-cm soil layer were used to derive the soil hydraulic properties that define the relationships of $\overline{z}_{WT}$ and root zone equilibrium moisture to catchment deficit (De Lannoy et al., 2014). That is, in the model the soil hydraulic parameters are assumed constant in the vertical dimension. In reality, soil texture and soil hydraulic parameters vary with depth. This is especially true in peatlands (Letts et al., 2000; McCarter & Price, 2014), where differentiation is typically made for two layers (acrotelm and catotelm) or for three layers (fibric, hemic, and sapric peat), not only for the saturated hydraulic conductivity profile described in section 2.2.2 but also for unsaturated hydraulic properties.

Since such a layered differentiation would not fit the overall CLSM structure, we decided to extract soil hydraulic parameters from an average acrotelm layer to represent the root zone, assuming that groundwater table fluctuations mostly occur in the acrotelm layer (down to a depth of −0.3 to −0.7 m; Ivanov, 1981). In so doing, we accept errors for anomalously dry situations in which the actual groundwater table would drop below the acrotelm-catotelm boundary. The updated parameter values for PEAT-CLSM are summarized in Table 2. Figure 3 shows a comparison of the hydraulic functions of PEAT-CLSM with the most frequently applied functions for the acrotelm of Letts et al. (2000; fibric and hemic peat) and functions determined in more recent works for the acrotelm layer of natural peatlands (Dettmann et al., 2014; McCarter & Price, 2014; Weber et al., 2017). Figure 3 indicates a large variability of hydraulic properties in the acrotelm layer; the green curves represent our attempt to represent this behavior in PEAT-CLSM with *average* relationships. Figure 3 also shows the peat properties introduced to CLSM by De Lannoy et al. (2014). These peat parameters were based on values from the Staring series (peat B16; Wösten et al., 2001), which are not representative of the acrotelm layer in natural peatlands. The samples of B16 were also taken from the top soil but likely included several degraded peat samples, as indicated by the bulk densities of B16 that ranged from 0.2 to 1.0 g/cm^3; these values exceed typical bulk densities of around 0.1 g/cm^3 found in undisturbed acrotelm layers (e.g., Nungesser, 2003).

2.2.4. Evapotranspiration

In earlier studies, the relative proportion of vascular plants and nonvascular plants (mosses) was considered crucial for modeling water, energy, and carbon cycles in peatlands (Dimitrov et al., 2011; Sonnentag et al., 2008). Mosses lack stomata to actively regulate their evaporative water loss, and they show an abrupt drying

Table 2
Overview of the Model Configurations, Land Model Parameters, and Boundary Conditions of the Simulation Experiments ExpA, ExpB, and ExpC

Simulation experiment	ExpA	ExpB	ExpC
CLSM Version	SMAP L4_SM Version 3	SMAP L4_SM Version 3	PEAT-CLSM
Peat soil	No	Yes	Yes
Soil hydraulic parameters	Textural input from NGDC (Reynolds et al., 2000), parameters adapted from Cosby et al. (1984) (as in MERRA-2)	$\theta_s = 0.80\ m^3/m^3$, $h_s = -1.76$ m, $b = 3.41$, $K_s = 7.86 \times 10^{-7}$ m/s, De Lannoy et al. (2014)	$\theta_s = 0.93\ m^3/m^3$, $h_s = -0.03$ m, $b = 3.5$, $K_s = 2.8 \times 10^{-5}$ m/s, and $K_{s,\mathrm{macro},z\,=\,0} = 10$ m/s
Topography/catchments	HYDRO1k (USGS)		No topography input used
Meteorological forcing	MERRA-2 (Gelaro et al., 2017) including gauge-based precipitation corrections (Reichle et al., 2017)		
Land cover	USGS Global Land Cover Characteristics Data Base Version 2.0 (GLCCv2), https://lta.cr.usgs.gov/glcc/		
Leaf area index (LAI)	Hybrid of Moderate Resolution Imaging Spectroradiometer (MODIS) and GEOLAND2 (Baret et al., 2013; Camacho et al., 2013)		
Greeness fraction	GSWP-2 (Dirmeyer & Oki, 2002)		
Albedo	Estimated by a modified Simple Biosphere Model (SiB) albedo parameterization scheme and (for the snow-free fraction) scaled by MODIS albedo climatology (Koster & Suarez, 1991; Moody, 2008)		

and decrease of productivity at certain groundwater table depths. The productivity of vascular plants, on the other hand, is relatively unaffected by groundwater table drawdown (Dimitrov et al., 2011; Strack et al., 2006). Though important, information on the relative proportion of plant species in peatlands is not available for global-scale applications.

Nearly all research on water-limited evapotranspiration (E) in peatlands has sought a link with groundwater depth ($\overline{z}_{\mathrm{WT}}$), but no unique relationship has been found (Lafleur, 2008). Whereas lysimeter studies indicate a strong relationship between E and $\overline{z}_{\mathrm{WT}}$ even at high $\overline{z}_{\mathrm{WT}}$ of −0.1 or −0.2 m (Schouwenaars, 1990; Virta, 1966), groundwater table effects are not clearly visible in field data (Peichl et al., 2013) or they occur at much lower $\overline{z}_{\mathrm{WT}}$ (of, e.g., −0.65 to −0.75 m; see Lafleur et al., 2005). This discrepancy is likely related to mechanisms of lateral evapotranspiration compensation at the field scale, such as enhanced E from vascular plants and open water bodies when E from mosses decreases during periods of lower $\overline{z}_{\mathrm{WT}}$ (Humphreys et al., 2006; Lafleur, 2008).

In designing PEAT-CLSM, we modified the evapotranspiration scheme of CLSM only with regard to the calculation of the areal wilting fraction, F_{wilt}. In CLSM, F_{wilt} is defined by the fraction of the spatial root zone soil moisture distribution that is at wilting point. Since in peatlands the groundwater table is typically in the

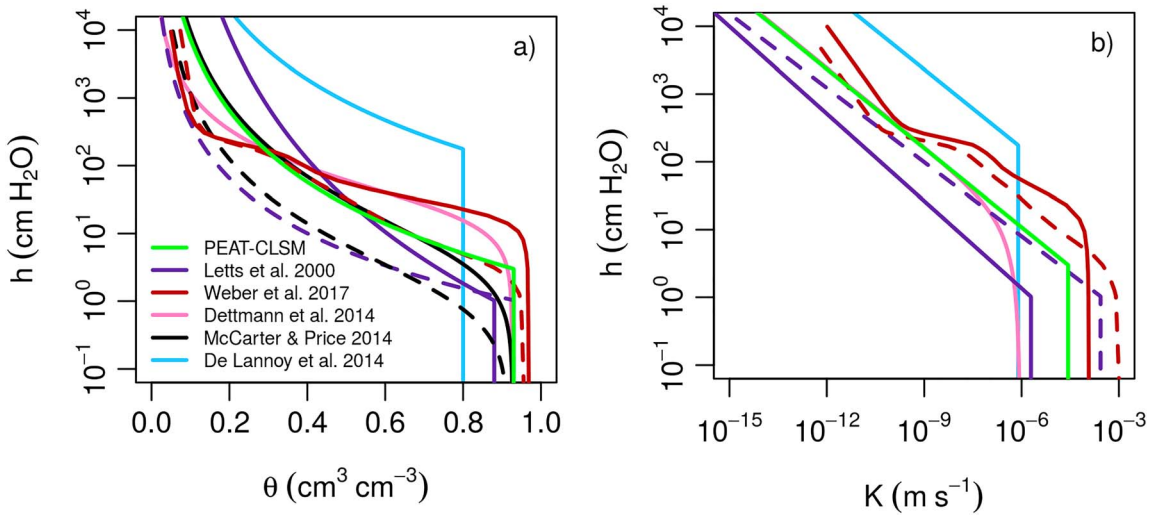

Figure 3. (a) Retention curves and (b) corresponding unsaturated hydraulic conductivity curves (if available) for the acrotelm peat layer from a range of studies (different colors), including the functions used in CLSM (De Lannoy et al., 2014) and PEAT-CLSM, with variables as explained in equations (4) and (5). Full lines pertain to average or deeper parts of the acrotelm, whereas dashed variants of the curves apply to shallower horizons within the acrotelm.

first meter, that is, always within the *root zone* of CLSM, this approach is inappropriate to describe peatland water stress. In PEAT-CLSM, we instead link F_{wilt} to $\bar{z}_{WT}$ as follows:

$$\begin{aligned} F_{wilt} &= 0.0 \quad for\ \bar{z}_{WT} \geq -0.3\,m \\ F_{wilt}(\bar{z}_{WT}) &= -0.3 - \bar{z}_{WT} \quad for -0.3\,m > \bar{z}_{WT} > -1.3\,m \\ F_{wilt} &= 1.0 \quad for\ \bar{z}_{WT} \leq -1.3\,m \end{aligned} \tag{10}$$

The choice of the thresholds for the initiation of water stress is based on lysimeter studies showing a water limitation for mosses at high $\bar{z}_{WT}$. The linear increase of F_{wilt} to 1 at $\bar{z}_{WT} = -1.3$ m was chosen to approximately mimic the reduction of E by 40% observed at Mer Bleue at lower $\bar{z}_{WT}$ of −0.65 to −0.75 m (Lafleur et al., 2005). Note that equation (10) is intended to determine the water-limited regime for an ecosystem of vascular and nonvascular plants as a whole. The parameterization of F_{wilt} is independent of the relative proportion of both plants due to the current lack of adequate global input.

3. Model Experimental Setup

3.1. Model Simulations

Three different suites of land surface simulations were conducted in this study. One suite of simulations (ExpA) used CLSM with default mineral soils globally. A second suite of simulations (ExpB) used CLSM with the updated soil parameterization of De Lannoy et al. (2014); this updated parameterization includes peat as a soil class. The third suite of simulations (ExpC) used PEAT-CLSM.

Details on the model configurations, land model parameters, and boundary conditions are given in Table 2. The basic model configuration was taken from the operational SMAP L4_SM product, version 3 (mimicked in ExpB; Reichle et al., 2018). For ExpA, we replaced the peat properties used for SMAP L4_SM by the mineral soil parameters that are still being used operationally for MERRA-2 (Reichle et al., 2017). In ExpC, we applied the PEAT-CLSM model changes, with the soil parameters listed in Table 2. The offline Richards simulations (section 2.1.1) were run separately for each set of soil parameters and used to obtain the corresponding land model moisture transfer coefficients for ExpA, ExpB, and ExpC. Other land model parameters and boundary conditions, including the surface meteorological forcing data, were the same across all simulations (Table 2).

Each simulation suite (ExpA through ExpC) was run for the period January 1988 through December 2017 and comprised simulations over two domains, each with its own spatial resolution: (1) a 9-km simulation for all grid cells between 40°N and 75°N that are dominated by peat soil according to a blend of Harmonized World Soil Data (HWSD-1.21) and the State Soil Geographic (STATSGO2) soil data (De Lannoy et al., 2014) and (2) a high-resolution 30″ (arc seconds) simulation only for those grid cells that contain field observations of groundwater table depth or evaporation (section 3.2). The latter simulation was done because some of the peatland in situ observations fall into 9-km grid cells where peat is not the dominant texture according to the blended soil map of De Lannoy et al. (2014). Therefore, for the simulations at 30″ resolution, we assigned peat soils (for ExpB and ExpC) and applied PEAT-CLSM (for ExpC) to all grid cells in the modeling domain. There are more recent and accurate maps of soil organic carbon, in particular WISE30sec (https://www.isric.org/index.php/explore/wise-databases) and the Northern Circumpolar Soil Carbon Database (https://bolin.su.se/data/ncscd), which could be used to define the model domain in future applications of PEAT-CLSM.

The 30″ simulations were run on a regular longitude-by-latitude grid, and the 9-skm simulations were run on the Equal Area Scalable Earth (EASE) grid, version 2.0. All simulations were preceded by multiple 37-year (whole MERRA-2 time series) spin-up cycles (separately for each experiment), with the final spin-up ending in December 1987.

3.2. Evaluation Approach

Figure 4 shows the spatial distribution of peat soils at 9-km resolution for North America, Europe, and Western Siberia according to De Lannoy et al. (2014). Long-term model estimates of hydrological variables over this domain will be evaluated qualitatively below. Figure 4 also shows the location of peatlands where extensive groundwater table depth ($\bar{z}_{WT}$) and evapotranspiration (E) data are available for detailed time

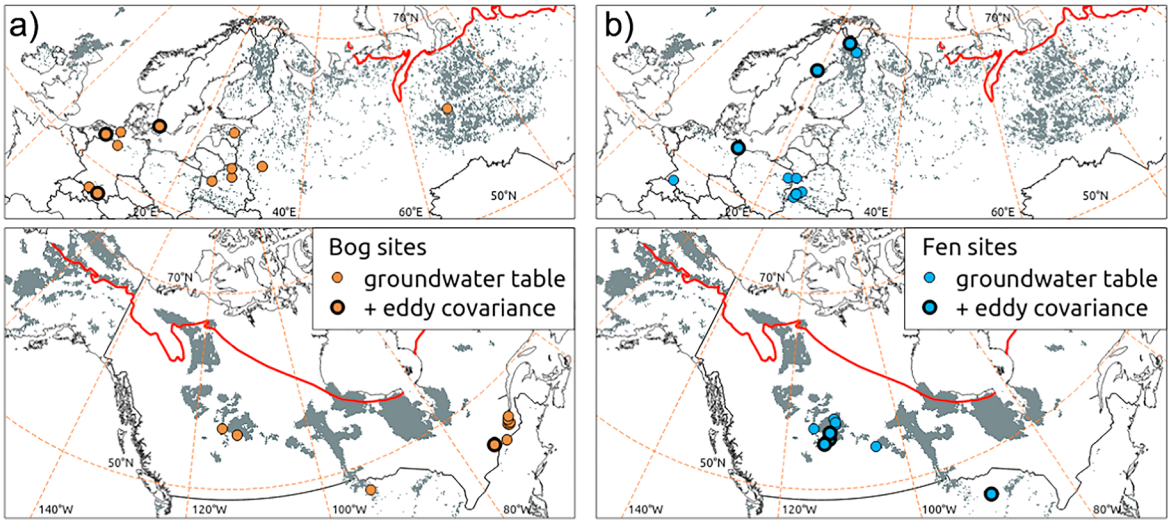

Figure 4. Distribution of (gray) peat soils in the temperate, boreal, and subarctic zone of the Northern Hemisphere based on De Lannoy et al. (2014), with the red line indicating the boundary of continuous permafrost (Brown et al., 1997). Markers locate peatland complexes (Table A1) with (filled circles) one or more groundwater table sites and (bold edge) additional eddy covariance data in (a) bogs and (b) fens.

series evaluation, over bogs (Figure 4a) and fens (Figure 4b). Due to the lack of sufficient hydrological field data, an evaluation for tropical peatlands is not conducted.

We compiled an extensive evaluation data set consisting of groundwater table depth observations in 94 monitoring wells in 44 different peatland complexes (22 bogs and 22 fens) and eddy covariance data with latent and sensible heat flux measurements from 11 different peatland complexes (4 bogs and 7 fens; Figure 4 and Table A1). Sites were chosen based upon the following criteria:

1. The presence of a peat layer with thickness >30 cm.
2. The peat being in a natural to seminatural state (1) without a history of intensive management that resulted in irreversibly disturbed peat properties and (2) with groundwater table depth fluctuations in the typical range for natural peatlands (0 to −0.5 m, sporadically deeper). The intensive management could refer to peat mining (though marginal peat cutting was accepted), deep drainage, and other attempts to change the land use for more than 10–20 years.
3. The monitoring well (for groundwater table depth sites) being perforated only over the first 1 or 2 m or with the perforated section of the tube ending within the peat layer. We emphasize that this criterion is particularly important because national authorities typically maintain only groundwater monitoring networks with monitoring wells that penetrate deeply and cut through the peat layer, producing observations that are not representative of the peat layer (Bechtold et al., 2014).

The temporal frequency of the groundwater table depth data ranged from daily (continuous logger data) to monthly (discontinuous manual measurements). When the data source provided information about the site-specific reference height for calculating the groundwater table depth, the site-specific reference height was, if necessary, shifted to the mean surface elevation to be consistent with the definition of $\overline{z}_{\mathrm{WT}}$ (equation (1)). If such information was not available, we assumed the mean surface elevation to be the reference height already. All field data were compared with daily averaged model output.

The latent heat flux measured by the eddy covariance method commonly underestimates the actual flux due to an incomplete energy balance. The gap in the energy balance closure is on average 24% for wetlands (Stoy et al., 2013). Therefore, a Bowen ratio preserving approach was applied to close the energy balance, following Mauder et al. (2013). The energy balance ratio, r_{RB}, was calculated as

$$r_{\mathrm{RB}} = \frac{H + \lambda E}{R_n + G} \tag{11}$$

where H is sensible heat flux (W/m^2) and λE is latent heat flux (W/m^2), with λ being the latent heat of vaporization. All nongap-filled half-hourly daytime (site data indicating net radiation R_n >20 W/m^2) values of each

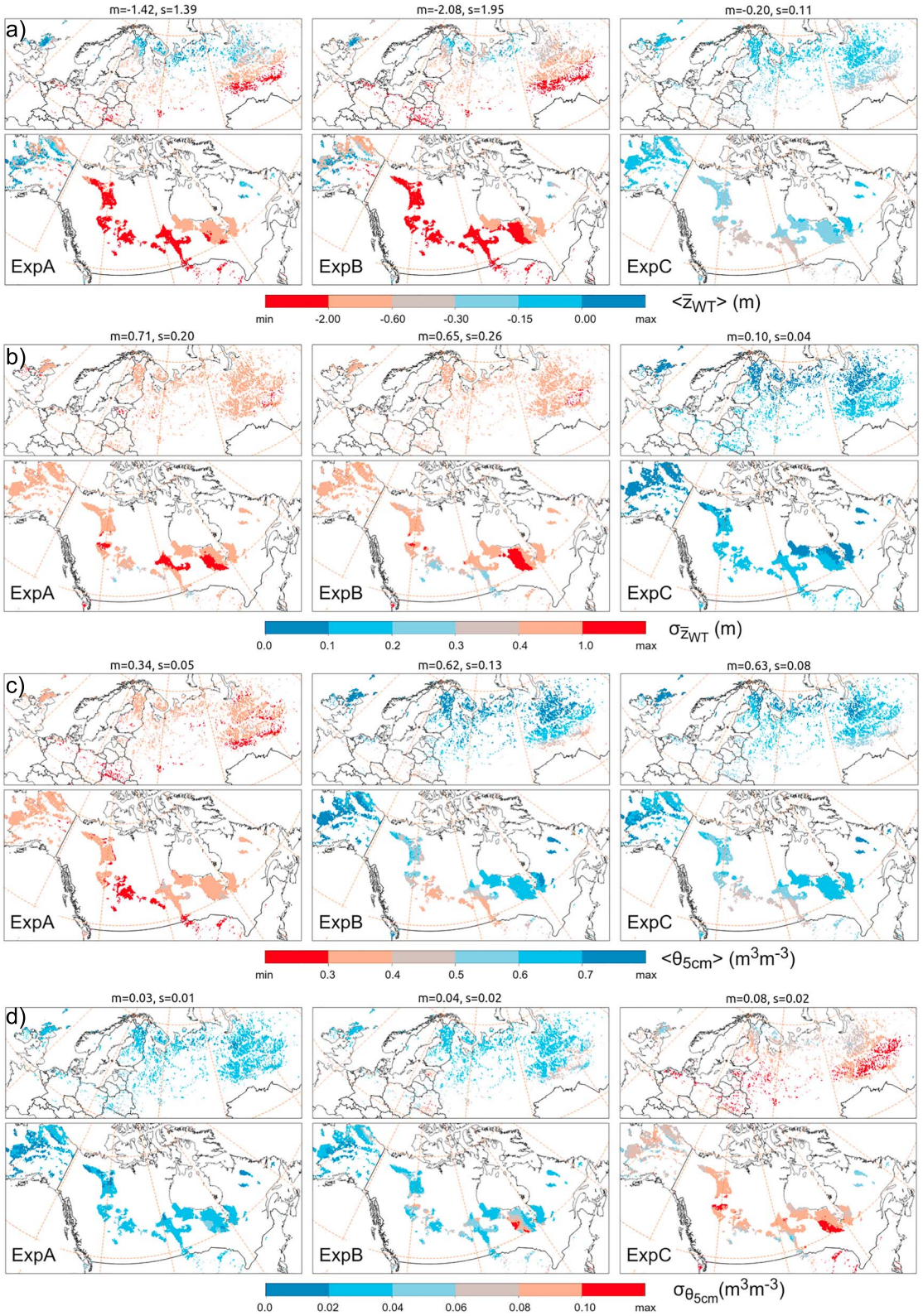

Figure 5. Long-term (1 January 1988 through 31 December 2017) (a) time-averaged spatial mean groundwater table depth (<$\bar{z}_{WT}$>), (b) temporal standard deviation of $\bar{z}_{WT}$ ($\sigma_{\bar{z}_{WT}}$), (c) time-averaged spatial mean volumetric soil moisture in the top 5 cm of the soil, <θ_{5cm}>, and (d) temporal standard deviation of θ_{5cm} ($\sigma_{\theta_{5cm}}$), for all three 9-km resolution simulations in ExpA, ExpB, and ExpC. Long-term statistics were computed with daily data from nonfrozen and snow-free periods. The titles include the spatial mean (m) and standard deviation (s) for 40°N to 75°N.

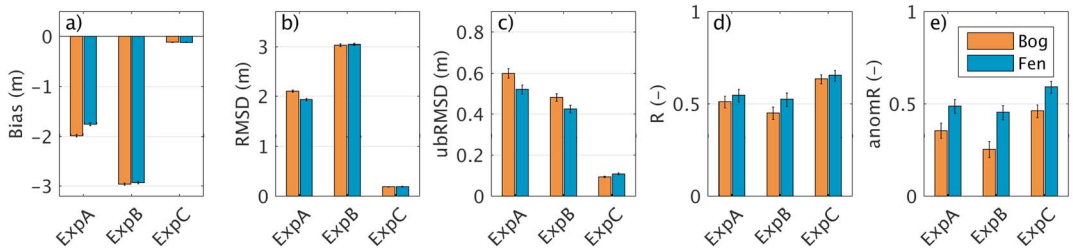

Figure 6. Groundwater table depth (a) bias (model-minus-observation), (b) root-mean-squared difference (RMSD), (c) unbiased root-mean-squared difference (ubRMSD), (d) time series correlation coefficient (R), and (e) anomaly time series correlation coefficient (anomR) for the 30″ simulations (ExpA, ExpB, and ExpC), computed separately for bogs and fens. Bog metrics are based on 55 sites collected into 14 regional clusters. Fen metrics are based on 39 sites collected into 11 regional clusters. The anomR metric is computed from slightly fewer sites (44 and 38, respectively, with 11 clusters each). The time period (1988–2017) varies per site depending on data availability and the length of snow and freezing periods, which were excluded. Also shown are 95% confidence intervals.

term on the right-hand side of equation (11) were averaged over a long moving window of 30 days to minimize the effects of storage change and of errors in soil heat flux measurements, G (W/m^2). For sites without measurements of G, estimates of G from a CLSM run (ExpB) were used. (The application of G from ExpA or ExpC instead of ExpB had an insignificant impact on the comparison of modeled and observed evapotranspiration rates.) The half-hourly H and λE values were corrected for the energy closure gap by multiplying them by $1/r_{\mathrm{RB}}$ for the corresponding 30-day window. The corrected eddy covariance half-hourly data were used without any gap-filling and aggregated to 3-hr averages. If a gap occurred over a 3-hr period, the average was discarded. In general, we restricted our comparison to rates of daytime evapotranspiration, E_{daytime}, for which nongap-filled data were available. Observed data were compared with 3-hourly averaged model output.

Skill metrics for groundwater table depth and evapotranspiration were only calculated for nonfrozen and snow-free periods. The observations spanned 1998 through 2017, though different time series lengths were available at different sites. We considered five metrics:

1. Bias: difference between simulated and observed long-term means (i.e., model minus observation)
2. RMSD: root-mean-square difference between simulated and observed time series
3. ubRMSD: unbiased root-mean-square difference, calculated by first removing the bias from the simulated time series
4. R: temporal Pearson correlation coefficient between observed and simulated data
5. anomR: temporal Pearson correlation coefficient between observed and simulated data, calculated after removing a multiyear (≥3 years), 30-day smoothed, seasonally varying mean from each time series, so that any correlation generated by the seasonality of the meteorological forcing is minimized. In this way the capability of the models to predict *unusual* interannual or short-term dynamics can be more directly evaluated. Only the midday 3-hr window was taken for the calculation of anomR of $\mathrm{E}_{\mathrm{daytime}}$.

The skill metrics are provided with 95% confidence intervals (CI), taking into account the temporal autocorrelation (as in De Lannoy & Reichle, 2016). Averaging of skill metrics and CIs occurred at two levels. First, they were averaged at the level of data clusters, which are defined by a minimum distance of 100 km—under the assumption that sites within a given cluster are not sufficiently independent from each other, site-specific skill metrics and CIs were averaged across the cluster by a simple mean (if applicable). Second, overall averages of skill metrics and CIs were computed across the cluster values. For the CI, the average was further divided by the square root of the number of clusters, under the assumption that each cluster added independent information.

4. Results and Discussion

4.1. Spatial Pattern of Groundwater Table Depth and Soil Moisture

Before evaluating the various experiment results against field observations, we compare their simulated spatial patterns of groundwater table depth and surface soil moisture (mean and standard deviation) over

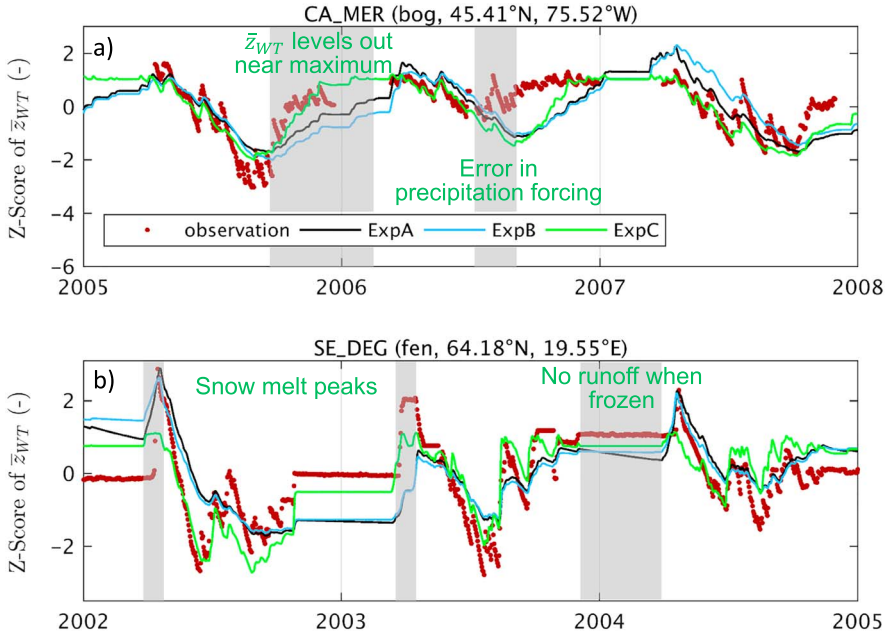

Figure 7. *Z*-transformed groundwater table depth ($\bar{z}_{WT}$) time series at (a) Mer Bleue (CA_MER) and (b) Degerö (SE_DEG). The tick for each year is located on 1 January. Shown are (red dots) field observations and 30″ simulations of (black) ExpA, (blue) ExpB, and (green) ExpC. The gray background marks some periods of interest (see text).

the main peatland regions of North America, Europe, and Western Siberia (Figure 5). Figure 5a shows that the long-term averaged $\bar{z}_{WT}$ ($<\bar{z}_{WT}>$) for ExpA and ExpB is generally lower than −0.6 m, with mean values of −1.42 m in ExpA and −2.08 m in ExpB. In contrast, ExpC shows values of $<\bar{z}_{WT}>$ that are in a realistic range for peatlands ($<\bar{z}_{WT}> > -0.6$ m). All simulations show a trend of higher $<\bar{z}_{WT}>$ values toward the north, reflecting the higher climatic water surplus at higher latitudes. Figure 5b also demonstrates that groundwater table fluctuations, that is, the temporal standard deviation of $\bar{z}_{WT}$ ($\sigma_{\bar{z}_{WT}}$), are more plausible in ExpC than they are in ExpA and ExpB; the average $\sigma_{\bar{z}_{WT}}$ in our in situ data set is 0.13 ± 0.07 m, which is fairly consistent with the standard deviations simulated by ExpC, whereas ExpA and ExpB always produce higher values. The relatively minor differences between ExpA and ExpB demonstrate the strong control of the *topographic index* distribution on groundwater table depth and base flow dynamics.

Figures 5c and 5d show the long-term mean and standard deviation of soil moisture. ExpA shows low soil moisture values with low variability, which is not unexpected given the use therein of mineral soils. ExpB, which uses a *peat soil* type, increases the soil moisture but largely maintains the temporal dynamics of ExpA. ExpC simulates on average a slightly drier and much more dynamic surface soil moisture compared to ExpB. This stems from the new peat soil hydraulic parameterization of PEAT-CLSM, which features a high fraction of pores that dewater between $h = 0$ cm H_2O and $h = -50$ cm H_2O (Figure 3), that is, dewater when $\bar{z}_{WT}$ fluctuates in that range.

Soil moisture field data of sufficient quality are not available in peatlands for a quantitative evaluation, but we can briefly discuss whether the changes seen in ExpC are sensible. One of the more sophisticated surface soil moisture data sets in peatlands can be found in Millard and Richardson (2018). They used a site-specific calibrated electromagnetic sensor to measure the surface soil moisture (top 5 cm) with a spatial interval of 1 m, covering the microtopography at several sites within a bog-fen complex. The observed surface soil moisture varied in time by about 0.2 m^3/m^3 at all sites. The high macroporosity in peatlands causes the acrotelm to dry out quickly when groundwater tables drop (Price, 1996). The very dynamical surface soil moisture is poorly represented by the hydraulic parameters of De Lannoy et al. (2014; ExpB), while the new hydraulic parameters, in particular the lower *b* parameter (see also Figure 3), in PEAT-CLSM (ExpC) results in a higher temporal standard deviation of surface soil moisture. The measured absolute surface soil moisture levels varied considerably across the sites of the study of Millard and Richardson (2018), with much drier values for bog sites (on average 0.3 to 0.35 m^3/m^3) than for fen sites (~0.6 m^3/m^3). The average surface

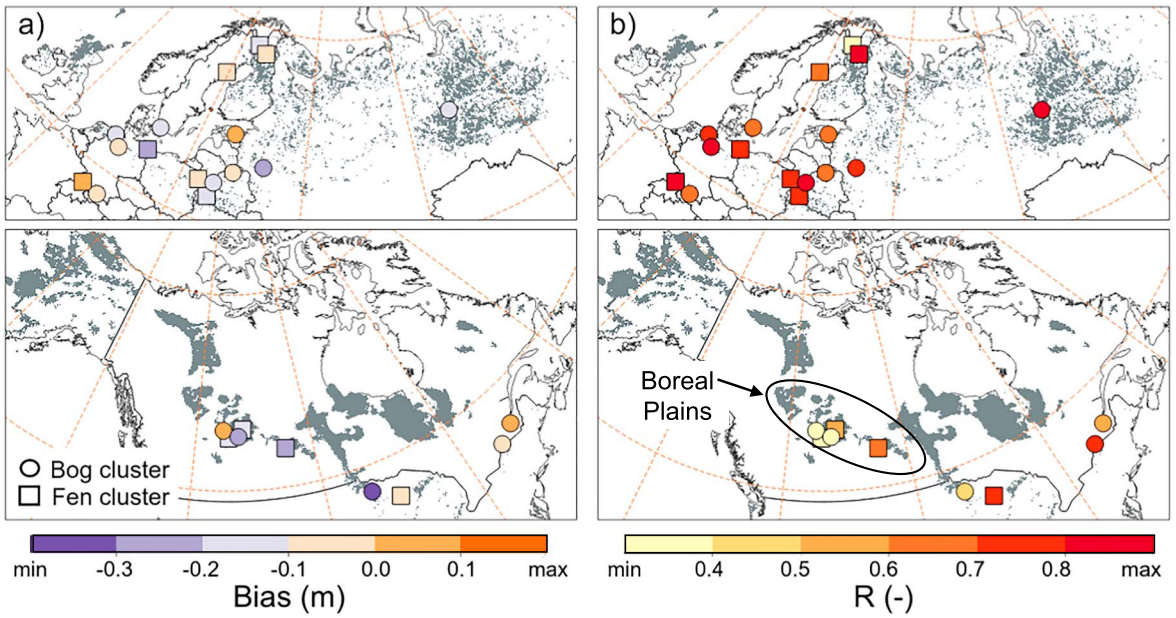

Figure 8. Long-term (a) bias and (b) correlation coefficient (*R*) in groundwater table depth for ExpC at each cluster of observational sites (underlying the data shown for ExpC in Figure 6). Circles indicate bog clusters, and squares indicate fen clusters.

soil moisture of ExpC (0.64 m^3/m^3) is higher than these values since PEAT-CLSM uses average acrotelm layer parameters that cannot reproduce the effect of decreasing *b* values toward the ground surface.

4.2. Groundwater Table Depth: Evaluation With Field Observations

Figure 6 summarizes the skill metrics of the 30″ simulations at the locations with in situ groundwater table depth data (Table A1) for bogs and fens. (Skill metrics computed, where possible, from the 9-km simulations are similar and are not shown.) Table A2 provides detailed skill metrics for each of the 94 groundwater table sites. The unrealistically low $\overline{z}_{WT}$ for ExpA and ExpB, along with their high standard deviations, lead to poor skill metrics for bias, RMSD, and ubRMSD (Figure 6). PEAT-CLSM (ExpC) improves on these statistics dramatically for both bogs and fens, with average values of −0.12, 0.19, and 0.10 m for bias, RMSD, and ubRMSD, respectively. The Pearson time series correlation coefficients (*R* and anomR) also improve significantly in ExpC, reaching respective values of 0.64 and 0.46 for bogs and 0.66 and 0.59 for fens. The TOPMODEL-based approach of CLSM (ExpA and ExpB) yields (significantly) greater *R* and anomR values for fens than for bogs, as one might expect given the dependence of fens on catchment hydrology. In that light, it is surprising that the simplified purely rain-fed approach of PEAT-CLSM (ExpC) yields equal *R* values for bogs and fens and significantly greater anomR values for fens than bogs.

We can only speculate about possible reasons for the lower performance of ExpC over bogs relative to the one over fens. One possibility is that the global forcing input (MERRA-2) is quite erroneous at the local scale. The impact of this on the water balance would be more problematic for smaller bogs than for fens, for which the water balance is associated with a larger area that helps average out forcing errors. Another possibility is that the effect of nonvascular plants on evapotranspiration, which is not specifically addressed in PEAT-CLSM, mainly causes difficulties in simulating the hydrology of bogs that typically show a higher proportion of nonvascular plants.

To illustrate the differences between the simulated groundwater table depth dynamics of ExpA, ExpB, and ExpC, portions of the observed and simulated time series at two representative and well-known sites, the Mer Bleue Bog (CA_MER) and Degerö Fen (SE_DEG) sites, are given in Figure 7. Time series were *Z*-transformed (centralized around the long-term mean and normalized by the long-term standard deviation) to correct for the huge bias in mean and standard deviation produced by ExpA and ExpB. The resulting dynamics in ExpA and ExpB, which are similar to each other, differ from those in ExpC (PEAT-CLSM). Figure 7a highlights a fundamental characteristic of a groundwater table time series in peatlands: the

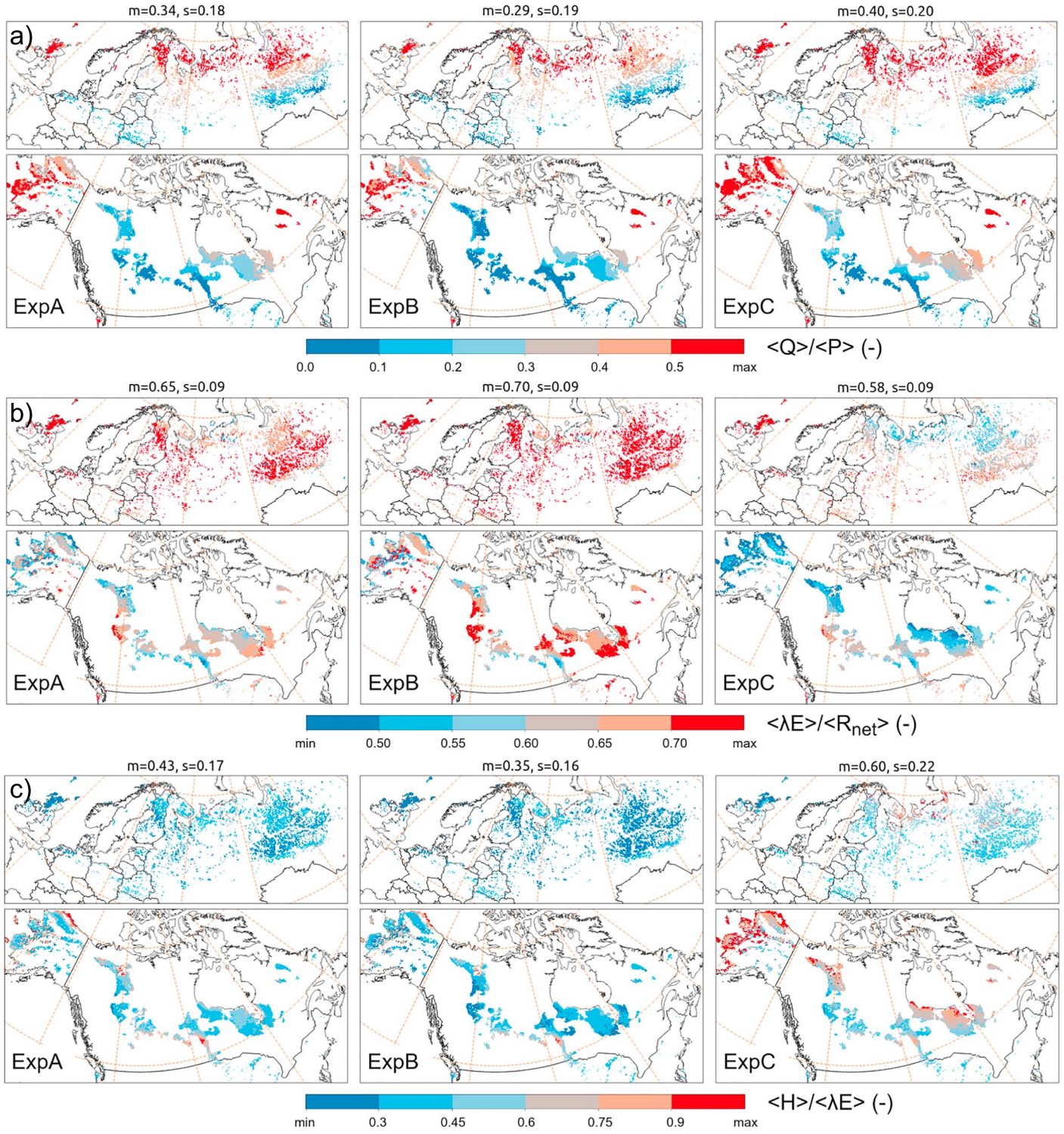

Figure 9. Long-term (1 January 1988 through 31 December 2017) (a) runoff efficiency (<*Q*>/<*P*>), (b) evapotranspiration efficiency (<*λE*>/<R_{net}>), and (c) Bowen ratio (<*H*>/<*λE*>) for all three 9-km resolution simulation experiments (ExpA, ExpB, and ExpC). (b) and (c) were computed with data from nonfrozen and snow-free periods. The titles provide the spatial mean (m) and standard deviation (s) for 40°N to 75°N.

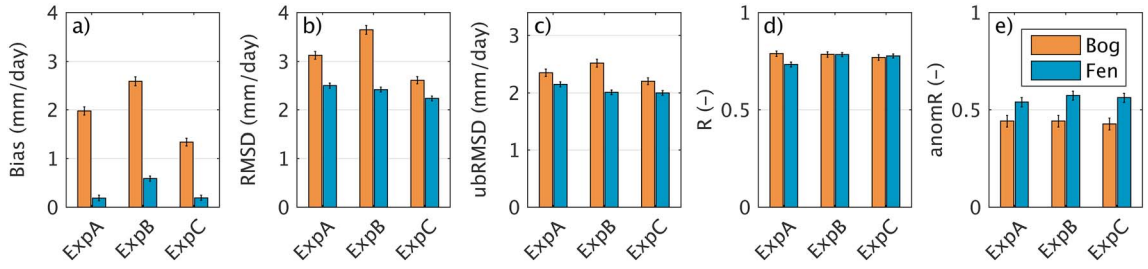

Figure 10. Daytime evapotranspiration rate (3-hourly resolution; mm/day) (a) bias (model-minus-observation), (b) root-mean-squared difference (RMSD), (c) unbiased root-mean-squared difference (ubRMSD), (d) time series correlation coefficient (R), and (e) anomaly time series correlation coefficient (anomR) for the 30″ simulations (ExpA, ExpB, and ExpC), computed separately for bogs and fens. Bog metrics are based on four sites. Fen metrics are based on seven sites. The anomR metric is based on two fewer fen sites. The time period (1988–2017) varies with site depending on data availability and the length of the snow and freezing periods, which were excluded. Also shown are 95% confidence intervals.

leveling out of groundwater tables when they approach their maximum, which corresponds approximately to the mean surface elevation. This feature is not captured in ExpA and ExpB but is very well reproduced by PEAT-CLSM for many sites, leading to high site-specific R values. (See Table A2. The R for the CA_MER site is 0.78.) The implementation of the microtopography approach and the exponential base flow function in PEAT-CLSM underlie this improvement. But Figure 7a also shows that at CA_MER simulated groundwater tables almost steadily decrease during midsummer 2006, whereas observed groundwater tables increase for this period. Precipitation measured at the site suggests storm events amounting to 116 mm of rain over 52 hr (31 July to 3 August 2006) were poorly represented by the coarse resolution of MERRA-2 and contributed to the discrepancy between observed and modeled groundwater table depths. Figure 7b (SE_DEG, $R = 0.68$) illustrates how groundwater tables in Nordic sites stabilize during freezing periods and peak after snowmelt. All simulations reproduce the timing and relative magnitude (after the Z-score transform) of these events reasonably well.

Figure 8 shows, for ExpC, a spatial map of the bias and correlation coefficient for ground groundwater tables over all observed bog and fen clusters. Europe and the Western Siberian Lowlands feature mostly high correlation coefficients and a moderate bias of −0.1 m. In North America, however, a deficiency of PEAT-CLSM is revealed by several clusters in the Boreal Plains and for one additional cluster lying southeast of there (supported by data from two US_S1 bog sites). The most negative biases (meaning that the modeled groundwater table is too low) and the lowest R values in that region are striking. Wetlands of the Boreal Plains are known for their specific hydrologic functioning that enabled peatland ecosystems to develop under a long-term regional climatic water deficit defined by an annual potential evapotranspiration that exceeds annual precipitation by 10% (Devito et al., 2012). These authors found that within deep heterogeneous glacial deposits characteristic of the Boreal Plains, water storage in large surface depressions in extensive clay-rich areas, as well as dynamic storage within local and more extensive groundwater flow systems, allows water surpluses in wetter years to provide water in drier years, potentially stabilizing regional groundwater tables (Hokanson et al., 2019; Lukenbach et al., 2017). Furthermore, negative feedback responses in peat soils and moss vegetation are more pronounced in continental boreal systems (Brown et al., 2010; Dixon et al., 2017; Waddington et al., 2015), and actual evapotranspiration rates of peatlands are likely lower in the Boreal Plains (Devito et al., 2017). Neither the long-term water storage memory in large depressions or groundwater flow systems nor the regionally specific evaporation rates are included in PEAT-CLSM, perhaps explaining the relatively poor model performance in the Boreal Plains.

4.3. Spatial Pattern of Runoff Efficiency, Evapotranspiration Efficiency, and Bowen Ratio

The water balance equation of a system without lateral water inputs and with negligible long-term water storage changes (features that typify natural bogs) reduces to

$$Q = P - E \tag{12}$$

where Q represents total runoff, P is the total precipitation, and E is evapotranspiration. Considering P as a driver of the system, the equation illustrates that long-term averages of Q and E are very highly coupled. For

the development of a land surface model, this means that a realistic simulation of long-term E requires realistic treatments of both E and Q (Koster, 2015).

We therefore jointly examine the long-term runoff and evapotranspiration fluxes for the main peatland regions between 40°N and 75°N. More specifically, Figure 9 shows the simulated spatial patterns of the 30-year runoff efficiency ($<Q>/<P>$; <.> indicating temporal means), evapotranspiration efficiency ($<\lambda E>/<R_{net}>$) and Bowen ratio ($<H>/<\lambda E>$) based on the 9-km simulations of ExpA, ExpB, and ExpC. Values of $<\lambda E>/<R_{net}>$ and $<H>/<\lambda E>$ were calculated for snow-free and unfrozen periods for consistency with reported literature values (Lafleur, 2008), whereas the calculation of runoff efficiency included snow and frozen periods given the importance of snowmelt water for runoff. ExpA and ExpB show similar patterns; both, though, show large differences with ExpC. In general, ExpC simulates higher $<Q>/<P>$ (more runoff), lower $<\lambda E>/<R_{net}>$ (less net radiation turned into evapotranspiration) and higher $<H>/<\lambda E>$ (more sensible heat). On average, runoff increased by 38% while evapotranspiration decreased by 19% in ExpC (relative to ExpB).

The lowest $<Q>/<P>$ (<0.1) values are seen over the Boreal Plains for all three simulation experiments (Figure 9a). This region is characterized by extremely low mean annual runoff fluxes from forest catchments and only slightly greater runoff from peatland-dominated catchments, with significant runoff generation occurring only about once every 20 years (Devito et al., 2005, 2017). The very low runoff amounts entail that equation (12) practically simplifies to E, which, in turn, leads to $<\lambda E>/<R_{net}>$ values that are rather similar for all experiments over the Boreal Plains (Figure 9b). For regions with higher $<Q>/<P>$, ExpC produces an evapotranspiration that is lower (and a runoff that is accordingly higher) than that in ExpA and ExpB. Consequently, $<H>/<\lambda E>$ is greater in ExpC, with values that increase from about 0.45 in the south of Canada and Russia to 0.75 at the permafrost boundary and with greater values further northward. Based on a literature review of field observations from sites between 45°N and 60°N and in New Zealand, Lafleur (2008) reported median Bowen ratios (in the growing season) of 0.60 for bogs and 0.46 for fens and mean evapotranspiration efficiencies that reach 0.46 for bogs and 0.59 for fens. Due to the strong influence of site-specific climatic conditions and measurement periods on observed evapotranspiration efficiency and Bowen ratio, it is impossible to determine which experiment agrees better with average literature values. Nevertheless, the results do indicate that PEAT-CLSM simulates flux ratios that are generally realistic.

4.4. Daytime Evapotranspiration: Evaluation With Field Observations

Figure 10 summarizes the skill metrics for evapotranspiration, computed separately for bogs and fens, based on the 30″ simulations performed at locations with evapotranspiration data (section 3.2 and Table A1). (Table A3 provides the detailed skill metrics for each of the 11 eddy covariance sites.) For bogs, ExpA, ExpB, and ExpC all overestimate daytime evapotranspiration rates ($E_{daytime}$), whereas for fens, the bias averaged over all sites is close to zero (Figure 10a). However, Table A3 indicates that large positive and negative biases do occur at individual fen sites. In field experiments, evapotranspiration efficiency has been reported to be about 25% lower in bogs than in fens (Lafleur, 2008), but this distinction was not achieved with the model simulations due to the lack of a bog-fen differentiation in CLSM and PEAT-CLSM, though we note that PEAT-CLSM (ExpC) does partly overcome the site-specific biases and reduces (relative to ExpB) the bias of $E_{daytime}$ for all bogs (on average by 50%) and for five of the seven fen sites. The bias reduction can be explained by considerable differences in the areal fractions of the hydrologic regimes, that is, F_{sat} and F_{wilt}, among ExpA, ExpB, and ExpC. PEAT-CLSM mostly simulated the lowest F_{sat} and highest F_{wilt} during summer, effectively reducing evapotranspiration (see Appendix B for exemplary time series). Besides bias reduction, ExpC further yields the lowest RMSD values for bogs and fens and the lowest ubRMSD for bogs. No significant differences in R and anomR are seen between the experiments.

5. Conclusions

In this paper, we introduce a peatland-specific land surface hydrology module (PEAT-CLSM) for the GEOS Catchment Land Surface Model (CLSM). In PEAT-CLSM, a characterization of microtopography is used to determine the groundwater table depth and soil moisture distributions, in contrast to the use of the catchment-scale compound topographic index distribution in CLSM. In addition, PEAT-CLSM features modified formulations of runoff and evapotranspiration and includes updated values of peat hydraulic

parameters. The parameterization was constructed from formulations and parameter values provided in the literature; it was not tuned in any way prior to its evaluation here against field measurements.

Three experiment suites were set up, all using similar global input data but different treatments of peatland. One experiment used default mineral soils in the original CLSM model (ExpA, representing the model used in MERRA-2), one used peat soil properties in the original CLSM model (ExpB, representing the model used for SMAP L4_SM), and the final experiment used revised peat soil properties within PEAT-CLSM (ExpC). An evaluation of simulated spatial patterns between 40°N and 75°N and a detailed evaluation against a newly compiled and extensive data set of observed groundwater table depths and evapotranspiration rates in natural and seminatural peatlands showed that

1. CLSM was unable to mimic typical groundwater table dynamics in peatlands, simulating groundwater table depths that are on average too deep below soil surface (< -1.0 m) and too variable (standard deviation >0.6 m);
2. simulated hydrological dynamics changed little from ExpA to ExpB, the only major change being an average increase of soil moisture from about 0.34 to 0.62 m^3/m^3;
3. PEAT-CLSM strongly modified the simulated hydrological dynamics, establishing a mean groundwater table depth of −0.20 m (during snow-free and unfrozen periods) with moderate temporal fluctuations (standard deviation of 0.10 m), and increasing runoff on average by 38% while reducing evapotranspiration by 19% relative to ExpB;
4. PEAT-CLSM agreed better than CLSM (using either MERRA-2 or SMAP L4_SM soil hydraulic parameters) with field observations of groundwater table depth, achieving a bias of −0.12 m, an unbiased RMSD of 0.1 m and a time series R of 0.65; and
5. PEAT-CLSM agreed better than CLSM (using either MERRA-2 or SMAP L4_SM soil hydraulic parameters) with evapotranspiration estimates from eddy covariance measurements, significantly reducing (relative to ExpB) the bias in daytime evapotranspiration for 9 of 11 peatland sites, which amounts to an average bias reduction of 1.3 mm/day for bogs and 0.4 mm/day for fens. Temporal correlation metrics did not change significantly.

The simplicity of the peatland-specific modifications to CLSM must be emphasized. PEAT-CLSM was purposely designed with a level of sophistication that, in effect, would allow its straightforward future incorporation into the modeling system underlying GEOS operational products such as MERRA-2 and SMAP L4_SM. Of course, such simplicity comes with shortcomings and caveats that could partly be overcome through the development of more sophisticated approaches.

First, in PEAT-CLSM, a *bog-type* modeling approach is used for all peatlands; lateral water input from ground or surface water is neglected. Even though skill metrics of PEAT-CLSM were similar for bogs and fens (and were even slightly superior for fens), a partial lateral water input (e.g., from upstream CLSM grid cells) could theoretically be implemented to further improve the performance for fens. The necessity of a more sophisticated approach is highlighted by the relatively poor skill metrics obtained over the Boreal Plains (Western Canada) where annual precipitation is very limited and lateral input (minerogenic and/or from adjacent peatlands) is an important stabilizing process. However, the parameterization of the lateral inputs is very difficult to constrain at regional to global scales. Even a harmonized global map indicating the relative proportion of bog and fen, which could be used as a first indication for the importance of lateral water input fluxes, does not yet exist.

A second shortcoming of PEAT-CLSM involves the evapotranspiration scheme, in particular the lack of accounting for the relative proportion of vascular and nonvascular plants. It is evident from the literature (Dimitrov et al., 2011; Gong et al., 2012; Lafleur, 2008) that a more sophisticated evapotranspiration scheme that is specifically designed for peatland vegetation could improve evapotranspiration estimates over peatlands in land surface models. In this paper, PEAT-CLSM used the LAI and greenness fraction from optical remote sensing data products along with the land cover classification of CLSM (an aggregated version of GLOBCOVER 2009; see Bontemps et al., 2011) with only six land cover types (Mahanama et al., 2015). When overlaid with the soil map, peat grid cells north of 40°N are mostly characterized by *needleleaf trees* and *grassland*, where the latter in effect represents a huge class lumping together all well-vegetated surfaces with low tree cover. A better stratification of vegetation is crucial for a better description of the spatial

heterogeneity of evapotranspiration over peatlands and over wetland areas in general (Lafleur, 2008). As peatland-specific processes gradually find their way into global land surface models, there is an exigency to improve the representation of peatlands in global land cover data sets.

A third shortcoming to consider is that in PEAT-CLSM, only the vertical gradient in $K_{s,\mathrm{macro}}$ is used in the base flow function; vertical gradients in all other hydraulic parameters are neglected. Unsaturated hydraulic properties are known to change gradually with depth over the acrotelm and from acrotelm to catotelm. Improvements in the vertical representation of soil hydrological processes have the potential to further improve peatland hydrology estimates.

Another process in peatlands that is known to be important but is not yet considered in PEAT-CLSM are peat volume changes due to swelling and shrinkage, along with the related vertical movements of the ground surface (Nijp et al., 2017; Whittington & Price, 2006). Furthermore, in PEAT-CLSM, all peatlands are treated as natural, that is, as undrained. Globally, drained peatlands emit large amounts of greenhouse gases (Tubiello et al., 2016). Thus, if the overall role played by peatlands in the global water and carbon cycles is to be modeled, the effects of drainage and dynamic land cover change accounting for the rapidly increasing area of drained tropical peatlands (Hooijer et al., 2010) need to be included.

Further progress in land surface modeling within GEOS involves merging PEAT-CLSM with the improved treatment of CLSM subsurface temperature dynamics developed by Tao et al. (2017). Moreover, the advances of PEAT-CLSM also need to be merged with the most recent CLSM updates of Version 4 of the L4_SM system (Reichle et al., 2018) and with the dynamic vegetation phenology version of CLSM (Koster & Walker, 2015). Our long-term development goal is to couple PEAT-CLSM to peatland-specific carbon cycle models.

Note that all improvements to the representation of peatland processes in global-scale land surface models will have to deal with a limited availability of spatial input information, given that in situ data collection in peatland regions is generally sparse. Remote sensing data are a potentially valuable resource in this regard, for they can constrain spatial patterns and time series of hydrological estimates by serving as ancillary input or as reference data for global parameter calibration. They can also contribute to dynamic surface water fraction estimation (Du et al., 2018) and to updating model variables via data assimilation (De Lannoy & Reichle, 2016). Future model development can benefit from incorporating such data.

Appendix A: Overview and Skill Metrics of Peatland Sites

A list with characteristics for all peatland sites used in the model evaluation is provided in Table A1. Detailed skill metrics for each of the sites is provided for water table depth in Table A2 and evapotranspiration in Table A3.

Appendix B: Exemplary Time Series of Evapotranspiration and Areal Fractions

Figure B1 uses time series of E_{daytime}, F_{sat}, and F_{wilt} to illustrate the mechanisms underlying the bias reduction achieved by PEAT-CLSM. The locations and time periods examined match those considered in Figure 7. For illustration purposes, E_{daytime} was aggregated to monthly averages; monthly averaged observations were obtained by averaging all available daytime 3-hourly data, and values for the simulations were obtained by averaging the simulation output over the corresponding time stamps. For both sites, E_{daytime} is overestimated by all the simulations, but the bias is nevertheless generally reduced in ExpC. The time series of the areal fractions of the hydrologic regimes, that is, F_{sat} and F_{wilt} (note that $F_{\mathrm{tra}} = 1 - F_{\mathrm{sat}} - F_{\mathrm{wilt}}$), show considerable differences between the experiments. PEAT-CLSM (ExpC) simulates the lowest F_{sat} at both sites over most of the summer, and it is the only model that simulated nonzero values of F_{wilt}. It can be seen that periods in which ExpC agrees better with site observations of E_{daytime} either coincide with periods in which it has the lowest F_{sat} values or with periods having significant values of F_{wilt}. The examples in Figure B1 illustrate that the fundamentally altered hydrological dynamics of PEAT-CLSM along with the imposed link between F_{wilt} and $\overline{z}_{\mathrm{WT}}$ effectively modulate the dynamics of E_{daytime}, leading to improvements in some skill metrics.

Journal of Advances in Modeling Earth Systems
10.1029/2018MS001574

Table A1
Overview of Peatland Sites (Grouped by Country and Alphabetically Sorted) With Groundwater Table Depth and Eddy Covariance (EC) Data That Were Used for Evaluation

Site code	Site/area name	Lat (°)	Lon (°)	# WT and period	# EC and period	*MAP (mm)	*MAT (°C)	Peatland type	Dominant vegetation	References
BY_berez_*	Rozhnianskaje	54.7554–54.7556	28.2806–28.2815	4[a] (2009–2013)	0	572	5.5	bog	Sphagnum mosses and spruce	n/a
BY_azery_*	Azery	53.8121–53.8229	24.2199–24.245	2[a] (2010–2013)	0	560	6.8	fen	Sphagnum mosses and spruce	
BY_svanets_aw	Zvaniec	52.033	24.8515	1[a] (2010–2012)	0	521	7.6	fen	Brown mosses and sedges	
BY_dok_log1.2	Dakudauskaje	53.7997	25.4426	1[a] (2012–2013)	0	568	6.4	bog	Sphagnum mosses and spruce	
BY_eig_f0910	Sparauskaje-Vysokaje	52.4011	25.0979	1[a] (2009–2013)	0	527	7.3	fen	Sphagnum mosses and spruce	
BY_sp_zdit_ghg	Sparauskaje-Zditava	52.4207	25.2703	1[a] (2010–2013)	0	527	7.3	fen	Sedges	
BY_scara_3	Scara	52.7876	25.7829	1[a] (2009–2013)	0	537	6.9	fen	Sedges	
BY_sp-pesch-p1	Sparauskaje-Pescanka	52.4516	25.0399	1[a] (2009–2013)	0	527	7.3	fen	Sedges and willows	
BY_sp_vy_p1	Sparauskaje-Vysokaje	52.4016	25.1029	1[a] (2009–2013)	0	527	7.3	fen	Sedges and willows	
BY_yelnia_*	Jelnia	55.5434–55.5732	27.8203–27.828	1[a] (2009–2013)	0	590	5.4	bog	Sphagnum mosses and spruce	
CA_FOM_PAUCI	Pauciflora Basin, Fort McMurray	56.3751	−111.2342	1[b] (2012–2017)	0	394	0.5	fen	Mosses, shrubs, sparse larches, and spruces	Wells et al. (2017)
CA_FOM_POP	Poplar Fen, Fort McMurray	56.9333	−111.5333	1[b] (2012–2017)	0	362	0.3	fen	Mosses, larches, and spruces	Elmes et al. (2018)
CA_FOM_SAL	Fort McMurray	56.5747	−111.2773	1[b] (2012–2017)	0	389	0.4	fen	Grasses, birches, and willows	Wells and Price (2015)
CA_MER	Mer Bleue	45.4094	−75.5186	1[c] (1998–2010)	1[c] (1998–2010)	735	6	bog	Mosses and shrubs	Lafleur et al. (2005)
CA_WP1	Canadian western peatland flux stations	54.9538	−112.467	1[d] (2003–2009)	1[d] (2004–2006)	336	2.4	fen	Trees, shrubs, and mosses	Flanagan and Syed (2011)
CA_WP2		55.5375	−112.3343	1[d] (2004–2006)	1[d] (2004–2006)	359	1.5	fen	Shrubs, grasses, and mosses	Adkinson et al. (2011)
CA_WP3		54.47	−113.32	1[d] (2004–2006)	1[d] (2004–2006)	364	3	fen	Grasses and mosses	Adkinson et al. (2011)
CA_SK_FEN	Sandhill fen, Saskatchewan	53.8021	−104.618	1[e] (2002–2016)	0	375	1.1	fen	Larches, shrubs, sedges, and mosses	Sonnentag et al. (2010)
CA_URSA_171_1	Utikuma Region Study Area	55.9809	−115.1885	1[f] (2008–2017)	0	388	1.8	bog	Spruce trees, shrubs, and mosses	Lukenbach et al. (2017)
CA_URSA_171_15	Utikuma Region Study Area	55.98	−115.19	1[f] (2011–2017)	0	388	1.8	fen	Spruce trees, shrubs, and mosses	Hokanson et al. (2016)
CA_WA_CTRL	Wandering River	55.3539	−112.5177	1[g] (2011–2013)	0	349	1.9	bog	Trees, shrubs, and mosses	Munir et al. (2015)
CA_LAW_SSE	Sainte-Séraphine, St. Lawrence	46.042	−72.345	1[h] (2014–2016)	0	817	5.4	bog	Mosses and shrubs	Bourgault et al. (2018)

Journal of Advances in Modeling Earth Systems 10.1029/2018MS001574

Table A1 *(continued)*

Site code	Site/area name	Lat (°)	Lon (°)	# WT and period	# EC and period	*MAP (mm)	*MAT (°C)	Peatland type	Dominant vegetation	References
	lowlands (LAW)									
CA_LAW_LCY	Lac Cyprès, LAW	45.95	−72.187	1[h] (2014–2016)	0	828	5.2	bog	Mosses and shrubs	
CA_LAW_VIC	Victoriaville, LAW	46.023	−72.077	1[h] (2014–2016)	0	829	5.1	bog	Mosses and shrubs	
CA_LAW_VR	Villeroy, LAW	46.376	−71.838	1[h] (2014–2016)	0	815	4.8	bog	Mosses, shrubs, and sedges	
CA_LAW_ISO	Issoudun, LAW	46.579	−71.597	1[h] (2014–2016)	0	807	4.5	bog	Mosses, shrubs, and sedges	
CA_LAW_CH	Covey Hill, LAW	45.008	−73.828	1[h] (2014–2016)	0	769	6.7	bog	Mosses, shrubs, and sedges	
DE_AF_*	Ahlenmoor	53.6859–53.6901	8.8272–8.8362	8[i] (2010–2016)	0	774	9.2	bog	Mosses, grasses, shrubs, and sparse birches	Frank et al. (2014) and Beetz et al. (2013)
DE_BM_*	Bourtanger Moor	52.6551–52.6559	7.1818–7.1839	5[i] (2011–2014)	1[i] (2011–2014)	750	9.5	bog	Mosses, shrubs, grasses, sparse birches, and pines	Hurkuck et al. (2014)
DE_SFS_*	Schechenfilz	47.81	11.33	5[i] (2010–2017)	1[j] (2010–2017)	967	7.9	bog	Mosses, pines, and shrubs	Hommeltenberg et al. (2014) and Dettmann and Bechtold (2016a)
DE_BIR_*	Birkenried	47.9473–47.9498	8.5741–8.5797	5[k] (2005–2007)	0	923	8.1	fen	Sedges and willows	n/a
DE_REM_K2	Kissleg	47.8227	9.9	1[k] (2010–2011)	0	975	8.4	bog	Mosses, shrubs, and pines	
DE_HMB_*	Bissendorfer Moor	52.4981–52.5037	9.663–9.6866	3[l] (2007–2009)	0	676	9.2	bog	Mosses and shrubs	n/a
DE_AKM_*	Anklam	53.8662–53.8665	13.6818–13.6834	2[i] (2010–2013)	1[m] (2010–2017)	592	8.7	fen	Willows, reed, and sedges	n/a
EE_MAE_kaev_*	Männikjärve	58.8773–58.8789	26.2163–26.2217	2[n] (2008–2016)	0	556	5	bog	Mosses, shrubs, grasses, and sparse dwarf pines	Burdun et al. (2019)
FI_HA	Halssiaapa	67.3686	26.6541	1[n] (2012–2016)	0	463	−0.6	fen	Mosses and sedges	Dinsmore et al. (2017)
FI_LOM	Lompolojänkkä	67.9972	24.2092	1[p] (2006–2017)	1[p] (2006–2016)	450	−0.8	fen	Willows, sedges, shrubs, and mosses	Aurela et al. (2009) and Aurela et al. (2015)
PL_BNP_*	Biebrza National Park	53.349–53.7123	22.5718–23.3642	12[q] (2009–2017)	0	548	7	fen	treeT, shrubs, and sedges	Grygoruk et al. (2011)
RU_MU_*	Mukhrino	60.8877–60.892	68.658–68.6837	4[r] (2009–2013)	0	468	−1.7	bog[+]	Mosses, sedges, shrubs, and dwarf trees	Bleuten and Filippov (2008)
RU_STA	Staroselsky Moch Hollow	56.474	33.04	1[s] (2013–2016)	0	612	4	bog	Mosses, sedges, and trees	Kurbatova et al. (2009)
SE_DEG	Degerö Stormyr	64.1833	19.55	1[t] (2001–2014)	1[t] (2001–2017)	555	2.1	fen		Peichl et al. (2013)

Journal of Advances in Modeling Earth Systems

10.1029/2018MS001574

Table A1 *(continued)*

Site code	Site/area name	Lat (°)	Lon (°)	# WT and period	# EC and period	*MAP (mm)	*MAT (°C)	Peatland type	Dominant vegetation	References
									Shrubs, sedges, and mosses	
SE_FAJ	Fäjemyr	56.2655	13.5535	1[u] (2006–2009)	1[u] (2005–2009)	775	7.4	bog	Shrubs, sedges, and mosses	Lund et al. (2012)
US_LOS	Lost Creek shrub fen	46.0827	−89.9792	1[v] (2000–2017)	1[v] (2000–2017)	656	4.7	fen	Trees, shrubs, and sedges	Sulman et al. (2009)
US_S1_*	S1 Bog of SPRUCE Project	47.5029	−93.4828	2[w] (2011–2013)	0	560	4.2	bog	Trees, shrubs, and mosses	Hanson et al. (2015)

Note. Sites of the same peatland complex were aggregated. Lat: latitude; Lon: longitude; #WT: number of groundwater table depth monitoring wells; #EC: number of eddy covariance sites; MAP: long-term mean annual MERRA-2 precipitation (1987–2017); MAT: long-term mean annual MERRA-2 air temperature (1987–2017). [+]bog-fen complex: Fen areas receive groundwater from raised ombrotrophic bog parts and not from mineral aquifers, which represents a specific scenario in the data set. All monitoring wells of RU_MU_* were treated as bogs in summary statistics. Data owner/source.

[a]University of Greifswald, Institute of Botany and Landscape Ecology, Germany (Annett Schneider) [b]Wetland Hydrology Lab, University of Waterloo, Canada [c]Carleton University, Trent University and McGill University, FLUXNET CANADA TEAM (2016) [d]Department of Biological Sciences, University of Lethbridge, Canada, FLUXNET CANADA TEAM (2016) [e]Garth van der Kamp (Environment Canada, Montreal); Global Institute for Water Security, University of Saskatchewan [f]Department of Biological Sciences, University of Alberta, Canada, HEAD RESEARCH [g]Tariq Munir, University of Calgary, Sun Gro Horticulture Canada [h]Marc André Bourgault, Université du Québec à Montréal [i]Thuenen Institute for Climate Smart Agriculture, Braunschweig, Germany [j]Institute for Meteorology and Climatology – -Atmospheric Environmental Research (IMK-IFU), Karlsruhe Institute of Technology (KIT), Garmisch-Partenkirchen, Germany [k]Markus Röhl Hochschule für Wirtschaft und Umwelt Nürtingen [l]Region Hannover [m]Thomas Gruenwald, Technische Universität Dresden, Institute of Hydrology and Meteorology, Tharandt, Germany [n]University of Tartu, Tooma mire research station [o]Finnish Meteorological Institute, http://litdb.fmi.fi/peatland.php [p]Annalea Lohila; Fluxnet; European fluxes database [q]Mateusz Grygoruk, Warsaw University of Life Sciences-SGGW, Faculty of Civil and Environmental Engineering [r]Wladimir Bleuten, Utrecht University, The Netherlands [s]Juliya Kurbatova, A. N. Severtsov Institute of Ecology and Evolution of Russian Academy of Sciences, Moscow, Russia [t]Mats B. Nilsson, Department of Forest Ecology and& Management, Swedish University of Agricultural Sciences, Sweden [u]Magnus Lund, European Fluxes Database Cluster [v]Ankur R. Desai, University of Wisconsin [w]Oak Ridge National Laboratory, https://mnspruce.ornl.gov/.

Journal of Advances in Modeling Earth Systems
10.1029/2018MS001574

Table A2
Skill Metrics for Groundwater Table Depth at the 94 Groundwater Table Sites

		BIAS (m)			RMSD (m)			ubRMSD (m)			*R* (−)			anomR (−)		
Site	Type	ExpA	ExpB	ExpC	ExpA	ExpB	ExpC	ExpA	ExpB	ExpC	ExpA	ExpB	ExpC	ExpA	ExpB	ExpC
BY_berez01	Bog	−0.86	−1.70	0.06	1.05	1.81	0.11	0.61	0.60	0.09	0.46	0.44	0.55	0.31	0.30	0.30
BY_berez03	Bog	−1.12	−1.97	−0.18	1.27	2.06	0.20	0.60	0.59	0.09	0.46	0.44	0.55	0.28	0.25	0.32
BY_berez04	Bog	−1.09	−1.94	−0.15	1.25	2.03	0.18	0.60	0.60	0.09	0.40	0.36	0.58	0.34	0.32	0.33
BY_berz02	Bog	−1.13	−1.98	−0.19	1.27	2.07	0.21	0.58	0.59	0.09	0.48	0.41	0.62	0.45	0.32	0.44
BY_dok_log1.2_l7752	Bog	−2.22	−3.42	−0.14	2.32	3.44	0.15	0.68	0.42	0.05	0.84	0.82	0.91	-	-	-
BY_yelnia-1	Bog	−1.47	−2.38	−0.13	1.61	2.43	0.15	0.68	0.48	0.08	0.81	0.66	0.81	0.52	0.08	0.72
BY_yelnia-2	Bog	−1.39	−2.31	−0.06	1.57	2.37	0.10	0.73	0.55	0.08	0.43	0.23	0.83	0.28	−0.16	0.69
BY_yelnia-3	Bog	−1.47	−2.38	−0.09	1.64	2.44	0.12	0.73	0.53	0.08	0.45	0.23	0.79	0.39	−0.09	0.65
BY_yelnia4	Bog	−1.07	−1.91	0.08	1.28	1.99	0.10	0.71	0.54	0.06	0.71	0.56	0.74	0.44	0.08	0.62
BY_yelnia5	Bog	−1.17	−2.01	−0.02	1.36	2.08	0.07	0.70	0.53	0.07	0.83	0.73	0.65	0.51	0.22	0.55
BY_yelnia6	Bog	−1.26	−2.10	−0.11	1.43	2.16	0.15	0.68	0.50	0.11	0.80	0.71	0.50	0.34	0.02	0.32
BY_yelnia-7	Bog	−1.22	−2.08	−0.12	1.39	2.14	0.16	0.67	0.52	0.11	0.73	0.50	0.68	0.57	0.00	0.63
BY_yelnia-8	Bog	−1.21	−2.06	−0.06	1.41	2.13	0.09	0.73	0.56	0.07	0.54	0.36	0.57	0.18	−0.20	0.29
BY_yelnia-9	Bog	−1.16	−2.01	−0.01	1.34	2.07	0.07	0.68	0.51	0.07	0.85	0.70	0.71	0.59	0.22	0.65
CA_LAW_CH	Bog	−0.77	−3.16	−0.16	0.80	3.18	0.19	0.22	0.29	0.10	0.75	0.80	0.72	-	-	-
CA_LAW_ISO	Bog	−0.74	−0.96	−0.04	0.95	1.15	0.07	0.59	0.64	0.06	0.38	0.37	0.32	-	-	-
CA_LAW_LCY	Bog	−1.16	−1.45	0.24	1.33	1.54	0.25	0.65	0.52	0.07	0.52	0.50	0.61	-	-	-
CA_LAW_SSE	Bog	−1.11	−1.60	0.21	1.31	1.69	0.22	0.70	0.54	0.06	0.40	0.35	0.70	-	-	-
CA_LAW_VIC	Bog	−1.26	−1.79	0.01	1.43	1.87	0.05	0.67	0.54	0.04	0.49	0.43	0.73	-	-	-
CA_LAW_VR	Bog	−0.99	−1.17	−0.03	1.13	1.28	0.05	0.54	0.52	0.04	0.17	0.13	0.59	-	-	-
CA_MER	Bog	−2.98	−3.79	0.01	3.20	3.83	0.10	1.17	0.55	0.10	0.64	0.57	0.78	0.59	0.46	0.68
CA_URSA_171_1	Bog	−1.77	−2.71	0.02	1.80	2.73	0.18	0.36	0.35	0.18	0.35	0.27	0.29	0.30	0.21	0.22
CA_WA_CTRL	Bog	−4.55	−6.53	−0.23	4.56	6.53	0.26	0.23	0.17	0.12	−0.14	−0.16	−0.07	−0.54	−0.56	−0.48
DE_AF_af_naturnah_sp	Bog	−1.73	−2.86	−0.22	1.86	2.91	0.23	0.70	0.52	0.09	0.55	0.44	0.77	0.47	0.33	0.67
DE_AF_af_noerd5seen_6041	Bog	−1.73	−2.86	−0.24	1.87	2.91	0.26	0.71	0.52	0.09	0.54	0.41	0.73	0.32	0.15	0.54
DE_AF_af_noerdhochfl_2415	Bog	−1.72	−2.86	−0.23	1.87	2.91	0.26	0.74	0.54	0.10	0.44	0.33	0.70	0.40	0.27	0.63
DE_AF_af_pegelwest_5432	Bog	−1.75	−2.83	−0.22	1.89	2.89	0.24	0.72	0.55	0.09	0.45	0.32	0.76	0.35	0.28	0.65
DE_AF_af_seepegel_5888	Bog	−1.67	−2.81	−0.19	1.81	2.85	0.21	0.71	0.52	0.09	0.50	0.39	0.78	0.43	0.30	0.68
DE_AF_af_siteam4_6043	Bog	−1.64	−2.72	−0.09	1.77	2.77	0.12	0.68	0.52	0.08	0.62	0.54	0.85	0.50	0.50	0.73
DE_AF_af_siteam5_5886	Bog	−1.64	−2.77	−0.15	1.79	2.82	0.18	0.71	0.52	0.09	0.50	0.41	0.75	0.40	0.31	0.64
DE_AF_af_siteam6_5899	Bog	−1.64	−2.72	−0.09	1.77	2.77	0.12	0.68	0.52	0.07	0.56	0.47	0.85	0.42	0.40	0.74
DE_BM	Bog	−3.43	−5.36	−0.20	3.47	5.37	0.23	0.48	0.32	0.11	0.37	0.31	0.62	0.17	0.14	0.48
DE_BM_bm_gw1_0579	Bog	−3.44	−5.37	−0.21	3.47	5.38	0.24	0.49	0.33	0.12	0.34	0.28	0.63	0.12	0.09	0.44
DE_BM_bm_gw3_0503	Bog	−3.41	−5.33	−0.18	3.44	5.34	0.21	0.48	0.32	0.11	0.38	0.31	0.64	0.15	0.12	0.45
DE_BM_bm_gw4_9837	Bog	−3.49	−5.42	−0.26	3.52	5.43	0.28	0.49	0.32	0.11	0.34	0.28	0.60	0.16	0.13	0.48
DE_BM_bm_gw5_0560	Bog	−3.30	−5.23	−0.07	3.34	5.24	0.13	0.48	0.32	0.11	0.40	0.33	0.67	0.19	0.15	0.50
DE_HMB_HM 83	Bog	−3.18	−5.46	0.24	3.24	5.47	0.26	0.62	0.31	0.10	0.78	0.74	0.92	-	-	-
DE_HMB_HM 94	Bog	−3.53	−5.81	−0.13	3.59	5.82	0.16	0.65	0.32	0.09	0.89	0.87	0.98	-	-	-
DE_HMB_HM 98	Bog	−3.68	−5.89	−0.15	3.72	5.89	0.18	0.55	0.26	0.10	0.84	0.83	0.91	-	-	-
DE_REM_K2	Bog	−1.18	−1.21	−0.06	1.31	1.31	0.08	0.56	0.50	0.06	0.26	0.15	0.75	-	-	-
DE_SF_mes_hang_ost_6012	Bog	−1.36	−1.94	−0.07	1.45	1.98	0.09	0.49	0.36	0.06	0.38	0.38	0.72	0.34	0.34	0.67
DE_SF_mes_hangwest_6267	Bog	−1.32	−1.85	−0.05	1.42	1.90	0.08	0.52	0.43	0.07	0.40	0.30	0.72	0.36	0.26	0.68
DE_SF_mes_logger_2407	Bog	−1.36	−1.87	−0.05	1.46	1.92	0.09	0.53	0.44	0.07	0.41	0.35	0.69	0.35	0.30	0.65
DE_SF_mes_site_diver_6025	Bog	−1.36	−1.90	−0.09	1.46	1.94	0.11	0.53	0.43	0.07	0.40	0.32	0.71	0.36	0.28	0.67
DE_SFS	Bog	−1.29	−1.82	−0.06	1.40	1.87	0.09	0.54	0.44	0.07	0.38	0.32	0.70	0.35	0.30	0.67
EE_MAE_kaev_222	Bog	−1.45	−2.18	0.07	1.74	2.30	0.13	0.97	0.74	0.11	0.44	0.29	0.63	0.50	0.25	0.65
EE_MAE_kaev_225	Bog	−1.56	−2.29	−0.05	1.84	2.40	0.11	0.96	0.73	0.10	0.51	0.34	0.70	0.49	0.24	0.67
RU_MU_H2	Bog	−1.02	−1.27	−0.03	1.18	1.37	0.06	0.59	0.52	0.05	0.80	0.78	0.84	0.81	0.76	0.82

Journal of Advances in Modeling Earth Systems
10.1029/2018MS001574

Table A2 *(continued)*

Site	Type	BIAS (m)			RMSD (m)			ubRMSD (m)			*R* (−)			anomR (−)		
		ExpA	ExpB	ExpC	ExpA	ExpB	ExpC	ExpA	ExpB	ExpC	ExpA	ExpB	ExpC	ExpA	ExpB	ExpC
RU_MU_H3	Bog	−1.00	−1.21	−0.10	1.17	1.32	0.11	0.61	0.54	0.05	0.87	0.89	0.87	0.88	0.90	0.86
RU_MU_H4	Bog	−0.88	−1.11	−0.08	1.02	1.19	0.09	0.51	0.44	0.05	0.90	0.93	0.78	0.77	0.81	0.75
RU_MU_H8	Bog	−1.14	−1.38	−0.21	1.29	1.48	0.22	0.60	0.54	0.05	0.83	0.83	0.85	0.73	0.74	0.80
RU_Staroselsky_Moch_Hollow	Bog	−1.70	−1.93	−0.23	1.84	2.04	0.25	0.69	0.66	0.09	0.56	0.32	0.79	0.53	0.31	0.73
SE_FAJ	Bog	−1.19	−1.53	−0.16	1.46	1.80	0.20	0.84	0.96	0.11	0.36	0.34	0.72	0.39	0.37	0.59
US_S1_EM1	Bog	−2.56	−3.62	−0.37	2.58	3.63	0.39	0.29	0.24	0.13	0.52	0.56	0.51	0.31	0.36	0.27
US_S1_EM2	Bog	−2.59	−3.65	−0.40	2.61	3.66	0.42	0.30	0.24	0.13	0.48	0.52	0.47	0.30	0.29	0.21
BY_d6992_azery	Fen	−2.48	−4.38	−0.26	2.58	4.40	0.29	0.68	0.39	0.12	0.85	0.87	0.58	0.90	0.92	0.61
BY_d7504_azery	Fen	−2.77	−4.61	−0.32	2.85	4.63	0.35	0.68	0.41	0.14	0.82	0.78	0.87	0.60	0.50	0.77
BY_d7523_svanets_aw	Fen	−3.25	−4.84	−0.32	3.27	4.85	0.33	0.39	0.25	0.07	0.84	0.82	0.79	0.54	0.53	0.63
BY_eig_f0910	Fen	−2.91	−5.42	−0.23	2.94	5.43	0.29	0.36	0.30	0.16	0.73	0.62	0.72	0.70	0.56	0.64
BY_f1020_sp_zdit_ghg	Fen	−3.02	−5.21	−0.11	3.05	5.22	0.23	0.42	0.18	0.20	0.90	0.88	0.77	0.85	0.84	0.64
BY_scara_3	Fen	−2.68	−4.50	0.29	2.75	4.52	0.30	0.64	0.37	0.09	0.67	0.64	0.75	-	-	-
BY_sp_vy_p1	Fen	−2.88	−5.39	−0.20	2.91	5.39	0.24	0.38	0.32	0.13	0.72	0.57	0.74	0.66	0.44	0.67
BY_sp-pesch-p1	Fen	−2.74	−5.20	−0.20	2.77	5.21	0.24	0.41	0.33	0.13	0.67	0.58	0.65	0.56	0.46	0.49
CA_FOM_PAUCI	Fen	−4.10	−6.17	−0.25	4.17	6.18	0.28	0.76	0.33	0.13	0.34	0.28	0.59	−0.01	−0.07	0.32
CA_FOM_POP	Fen	−2.87	−5.23	−0.28	2.88	5.23	0.30	0.30	0.26	0.12	0.56	0.55	0.58	0.65	0.61	0.73
CA_FOM_SAL	Fen	−3.90	−6.00	−0.22	3.94	6.01	0.28	0.56	0.38	0.18	0.00	−0.09	0.38	−0.20	−0.27	0.24
CA_SK_FEN	Fen	−1.59	−3.06	−0.23	1.62	3.07	0.28	0.28	0.28	0.15	0.28	0.42	0.64	0.41	0.53	0.71
CA_URSA_171_15	Fen	−1.89	−2.76	−0.09	1.91	2.77	0.16	0.31	0.29	0.13	0.57	0.48	0.51	0.08	−0.07	0.15
CA_WP1	Fen	−3.42	−4.49	−0.15	3.43	4.49	0.20	0.27	0.17	0.12	0.32	0.40	0.46	0.45	0.57	0.66
CA_WP2	Fen	−4.55	−6.68	−0.09	4.56	6.68	0.13	0.26	0.16	0.09	0.48	0.30	0.61	0.34	0.06	0.57
CA_WP3	Fen	−2.49	−3.17	−0.24	2.52	3.17	0.26	0.33	0.16	0.10	0.37	0.36	0.25	0.59	0.64	0.57
DE_AKM	Fen	−2.37	−4.76	−0.23	2.45	4.77	0.26	0.64	0.37	0.11	0.42	0.20	0.72	0.26	−0.07	0.53
DE_AKM_PEA_ak_r2_p1	Fen	−2.26	−4.69	−0.18	2.36	4.71	0.20	0.68	0.35	0.10	0.49	0.32	0.73	0.34	0.07	0.52
DE_BIR_P10	Fen	−1.33	−1.69	0.09	1.68	1.74	0.10	1.03	0.40	0.05	0.83	0.75	0.95	0.70	0.68	0.84
DE_BIR_P11	Fen	−1.36	−1.72	0.06	1.70	1.76	0.07	1.03	0.40	0.04	0.85	0.77	0.96	0.67	0.60	0.87
DE_BIR_P13	Fen	−1.59	−1.90	−0.10	1.89	1.95	0.12	1.04	0.41	0.05	0.83	0.73	0.90	0.58	0.51	0.58
DE_BIR_P8	Fen	−1.23	−1.61	0.04	1.58	1.65	0.11	0.99	0.40	0.10	0.80	0.72	0.90	0.64	0.65	0.78
DE_BIR_P9	Fen	−1.23	−1.61	0.03	1.61	1.67	0.07	1.03	0.43	0.06	0.85	0.78	0.87	0.70	0.66	0.80
FI_HA	Fen	0.00	−0.20	−0.07	0.50	0.56	0.08	0.50	0.53	0.04	0.70	0.74	0.82	0.80	0.81	0.77
FI_LOM	Fen	−0.07	−0.18	−0.14	0.49	0.57	0.15	0.49	0.54	0.05	0.25	0.25	0.29	0.23	0.21	0.23
PL_BPN_126	Fen	−1.90	−2.89	−0.14	1.94	2.91	0.26	0.41	0.31	0.22	0.62	0.71	0.74	0.47	0.61	0.65
PL_BPN_144	Fen	−2.14	−3.30	0.11	2.17	3.31	0.26	0.37	0.25	0.23	0.74	0.82	0.82	0.63	0.74	0.76
PL_BPN_151	Fen	−2.32	−3.69	−0.04	2.35	3.70	0.18	0.37	0.23	0.17	0.77	0.85	0.88	0.61	0.75	0.83
PL_BPN_154	Fen	−2.53	−4.31	−0.16	2.65	4.34	0.18	0.77	0.51	0.08	0.68	0.62	0.78	0.64	0.56	0.77
PL_BPN_162	Fen	−2.04	−3.06	−0.28	2.09	3.08	0.30	0.46	0.35	0.10	0.57	0.73	0.79	0.51	0.68	0.78
PL_BPN_177	Fen	−2.34	−3.63	−0.07	2.37	3.64	0.21	0.38	0.24	0.20	0.72	0.82	0.82	0.57	0.72	0.76
PL_BPN_179	Fen	−2.52	−3.93	0.00	2.56	3.94	0.17	0.45	0.30	0.17	0.66	0.76	0.73	0.53	0.67	0.62
PL_BPN_185	Fen	−2.55	−3.84	−0.07	2.57	3.84	0.18	0.35	0.23	0.17	0.77	0.83	0.90	0.61	0.70	0.83
PL_BPN_189	Fen	−2.34	−3.64	0.02	2.37	3.65	0.16	0.37	0.29	0.16	0.83	0.79	0.86	0.73	0.70	0.81
PL_BPN_191	Fen	−2.62	−4.06	−0.17	2.66	4.08	0.22	0.43	0.31	0.15	0.67	0.73	0.80	0.55	0.65	0.77
PL_BPN_208	Fen	−2.44	−3.51	−0.11	2.45	3.51	0.22	0.20	0.17	0.19	0.75	0.79	0.82	0.82	0.87	0.86
PL_BPN_212	Fen	−2.08	−3.11	0.19	2.09	3.11	0.30	0.23	0.20	0.24	0.76	0.80	0.79	0.70	0.77	0.73
SE_DEG	Fen	−0.31	−0.49	0.00	0.65	0.80	0.07	0.57	0.63	0.07	0.56	0.58	0.68	0.44	0.47	0.60
US_LOS	Fen	−2.5	−4.4	−0	2.55	4.45	0.18	0.58	0.85	0.18	0.65	0.6	0.71	0.66	0.61	0.73

Table A3
Skill Metrics for 3-Hourly Daytime Evapotranspiration Rates (mm/day) at the 11 Eddy Covariance Sites

	Type	BIAS (mm/day)			RMSD (mm/day)			ubRMSD (mm/day)			*R* (−)			anomR (−)		
Site		ExpA	ExpB	ExpC	ExpA	ExpB	ExpC	ExpA	ExpB	ExpC	ExpA	ExpB	ExpC	ExpA	ExpB	ExpC
CA_MER	Bog	1.5	2.4	1.1	2.6	3.4	2.5	2.2	2.4	2.2	0.86	0.86	0.84	0.61	0.62	0.59
DE_BM	Bog	1.9	2.4	1.1	2.9	3.4	2.5	2.3	2.4	2.2	0.75	0.75	0.69	0.23	0.23	0.19
DE_SFS	Bog	1.1	1.6	0.9	2.6	3.0	2.5	2.4	2.5	2.3	0.79	0.79	0.80	0.37	0.37	0.38
SE_FAJ	Bog	3.5	3.9	2.0	4.4	4.9	2.9	2.6	2.9	2.0	0.75	0.75	0.75	0.56	0.55	0.55
Average	Bog	2.0	2.6	1.3	3.1	3.6	2.6	2.4	2.5	2.2	0.79	0.79	0.77	0.44	0.44	0.43
Mean absolute bias	Bog	2.0	2.6	1.3	-	-	-	-	-	-	-	-	-	-	-	-
CA_WP1	Fen	−1.6	−1.2	−0.9	2.8	2.3	1.9	2.4	1.9	1.7	0.74	0.84	0.88	0.37	0.53	0.61
CA_WP2	Fen	−1.3	−1.1	−1.0	2.4	2.3	2.3	2.1	2.0	2.1	0.79	0.80	0.80	-	-	-
CA_WP3	Fen	−0.4	0.3	0.9	2.4	1.8	2.0	2.4	1.8	1.8	0.55	0.76	0.82	-	-	-
DE_AKM	Fen	−0.2	0.4	−0.9	2.0	1.9	2.4	2.0	1.9	2.2	0.81	0.83	0.75	0.56	0.58	0.47
FI_LOM	Fen	1.0	1.2	0.3	1.9	2.0	1.6	1.6	1.7	1.6	0.75	0.75	0.73	0.69	0.69	0.71
SE_DEG	Fen	1.9	2.2	0.9	2.8	3.1	2.1	2.0	2.1	1.9	0.66	0.66	0.63	0.52	0.51	0.52
US_LOS	Fen	1.8	2.3	1.9	3.2	3.5	3.3	2.6	2.6	2.7	0.84	0.86	0.84	0.56	0.56	0.51
Average	Fen	0.2	0.6	0.2	2.5	2.4	2.2	2.1	2.0	2.0	0.73	0.79	0.78	0.54	0.57	0.56
Mean absolute bias	Fen	1.2	1.2	1.0	-	-	-	-	-	-	-	-	-	-	-	-

Note. For the bias, the best model is underlined for each site.

Acknowledgments
M. Bechtold thanks the Alexander von Humboldt Foundation for a Feodor Lynen Fellowship. Use of High-Performance Computing infrastructure was funded by FWO-1512817N. R. Reichle and R. Koster were supported by the NASA Modeling, Analysis, and Prediction program. We thank Nigel Roulet and one anonymous reviewer for their very thorough and excellent reviews. Groundwater table and eddy covariance data used in this study are available at the sources indicated in Table A1. Complete simulation output for all evaluation sites (3-hourly resolution) and reduced simulation output for all Northern peatlands (30-year averages and daily resolution for 1988, 9-km EASEv2 grid) are available at https://doi.org/10.17605/OSF.IO/E58YM. Full simulation output (Northern peatlands) can be obtained from the authors upon request. This work used eddy covariance data acquired and shared by the FLUXNET community. The FLUXNET eddy covariance data processing and harmonization were carried out by the European Fluxes Database Cluster, AmeriFlux Management Project, and Fluxdata project of FLUXNET, with the support of CDIAC and ICOS Ecosystem Thematic Center, and the OzFlux, ChinaFlux, and AsiaFlux offices. Conversations with Dirk Roose on model development and the project of the Feodor Lynen Fellowship are greatly appreciated. We also acknowledge the following sources and investigators for supplying data: Mika Aurela, Larry Flanagan, Miriam Hurkuck, Eric Kessel, Peter Lafleur,

References

Adkinson, A. C., Syed, K. H., & Flanagan, L. B. (2011). Contrasting responses of growing season ecosystem CO_2 exchange to variation in temperature and water table depth in two peatlands in northern Alberta, Canada. *Journal of Geophysical Research*, *116*, G01004. https://doi.org/10.1029/2010JG001512

Aurela, M., Lohila, A., Tuovinen, J. P., Hatakka, J., Riutta, T., & Laurila, T. (2009). Carbon dioxide exchange on a northern boreal fen. *Boreal Environment Research*, *29*(4), 461–481. https://doi.org/10.1093/treephys/tpn047

Aurela, M., Lohila, A., Tuovinen, J.-P., Hatakka, J., Penttilä, T., & Laurila, T. (2015). Carbon dioxide and energy flux measurements in four northern-boreal ecosystems at Pallas. *Boreal Environment Research*, *20*, 455–473.

Baird, A. J. (1997). Field estimation of macropore functioning and surface hydraulic conductivity in a fen peat. *Hydrological Processes*, *11*(3), 287–295. https://doi.org/10.1002/(SICI)1099-1085(19970315)11:3<287::AID-HYP443>3.0.CO;2-L

Balsamo, G., Beljaars, A., Scipal, K., Viterbo, P., van den Hurk, B., Hirschi, M., & Betts, A. K. (2009). A revised hydrology for the ECMWF model: Verification from field site to terrestrial water storage and impact in the integrated forecast system. *Journal of Hydrometeorology*, *10*(3), 623–643. https://doi.org/10.1175/2008JHM1068.1

Baret, F., Weiss, M., Lacaze, R., Camacho, F., Makhmara, H., Pacholcyzk, P., & Smets, B. (2013). GEOV1: LAI and FAPAR essential climate variables and FCOVER global time series capitalizing over existing products. Part1: Principles of development and production.. *Remote Sensing of Environment*, *137*, 299–309. https://doi.org/10.1016/j.rse.2012.12.027

Bechtold, M., Tiemeyer, B., Laggner, A., Leppelt, T., Frahm, E., & Belting, S. (2014). Large-scale regionalization of water table depth in peatlands optimized for greenhouse gas emission upscaling. *Hydrology and Earth System Sciences*, *18*(9), 3319–3339. https://doi.org/10.5194/hess-18-3319-2014

Beetz, S., Liebersbach, H., Glatzel, S., Jurasinski, G., Buczko, U., & Höper, H. (2013). Effects of land use intensity on the full greenhouse gas balance in an Atlantic peat bog. *Biogeosciences*, *10*(2), 1067–1082. https://doi.org/10.5194/bg-10-1067-2013

Belyea, L. R., & Baird, A. J. (2006). Beyond "the limits to peat bog growth": Cross-scale feedback in peatland development. *Ecological Monographs*, *76*(3), 299–322. https://doi.org/https://doi.org/10.1890/0012-9615(2006)076[0299:BTLTPB]2.0.CO;2

Beven, K. J., & Kirkby, M. J. (1979). Towards a simple, physically based, variable contributing area model of catchment hydrology. *Bulletin of the International Association of Scientific Hydrology*, *24*, 43–69.

Bleuten, W., & Filippov, I. (2008). Hydrology of mire ecosystems in central West Siberia: The Mukhrino field station. In M. V. Glagolev, & E. D. Lapshina (Eds.), *Transactions of Unesco Department of Yugorsky State University "Dynamics of environment and global climate change"*, (Vol. 1, pp. 208–224). Novosibirsk: NSU.

Bohn, T. J., Podest, E., Schroeder, R., Pinto, N., McDonald, K. C., Glagolev, M., et al. (2013). Modeling the large-scale effects of surface moisture heterogeneity on wetland carbon fluxes in the West Siberian Lowland. *Biogeosciences*, *10*(10), 6559–6576. https://doi.org/10.5194/bg-10-6559-2013

Bontemps, S., Defourny, P., van Bogaert, E., Kalogirou, V., & Perez, J. R. (2011). GLOBCOVER 2009 products description and validation report. ESA Bulletin https://doi.org/10013/epic.39884.d016

Borren, W., & Bleuten, W. (2006). Simulating Holocene carbon accumulation in a western Siberian watershed mire using a three-dimensional dynamic modeling approach. *Water Resources Research*, *42*, W12413. https://doi.org/10.1029/2006WR004885

Bourgault, M.-A., Larocque, M., Garneau, M., & Roux, M. (2018). Quantifying peat hydrodynamic properties and their influence on water table depths in peatlands of southern Quebec (Canada). *Ecohydrology*, *11*(7), 1–12. https://doi.org/10.1002/eco.1976

Brown, J., Ferrians, O. J. Jr, Heginbottom, J. A., & Melnikov, E. S. (1997). Circum-Arctic map of permafrost and ground-ice conditions (Circum-Pacific Map Series CP-45, scale 1:10,000,000, 1 sheet). Retrieved from https://doi.org/10.3133/cp45

Brown, S. M., Petrone, R. M., Mendoza, C., & Devito, K. J. (2010). Surface vegetation controls on evapotranspiration from a sub-humid Western Boreal Plain wetland. *Hydrological Processes*, *24*(8), 1072–1085. https://doi.org/10.1002/hyp.7569

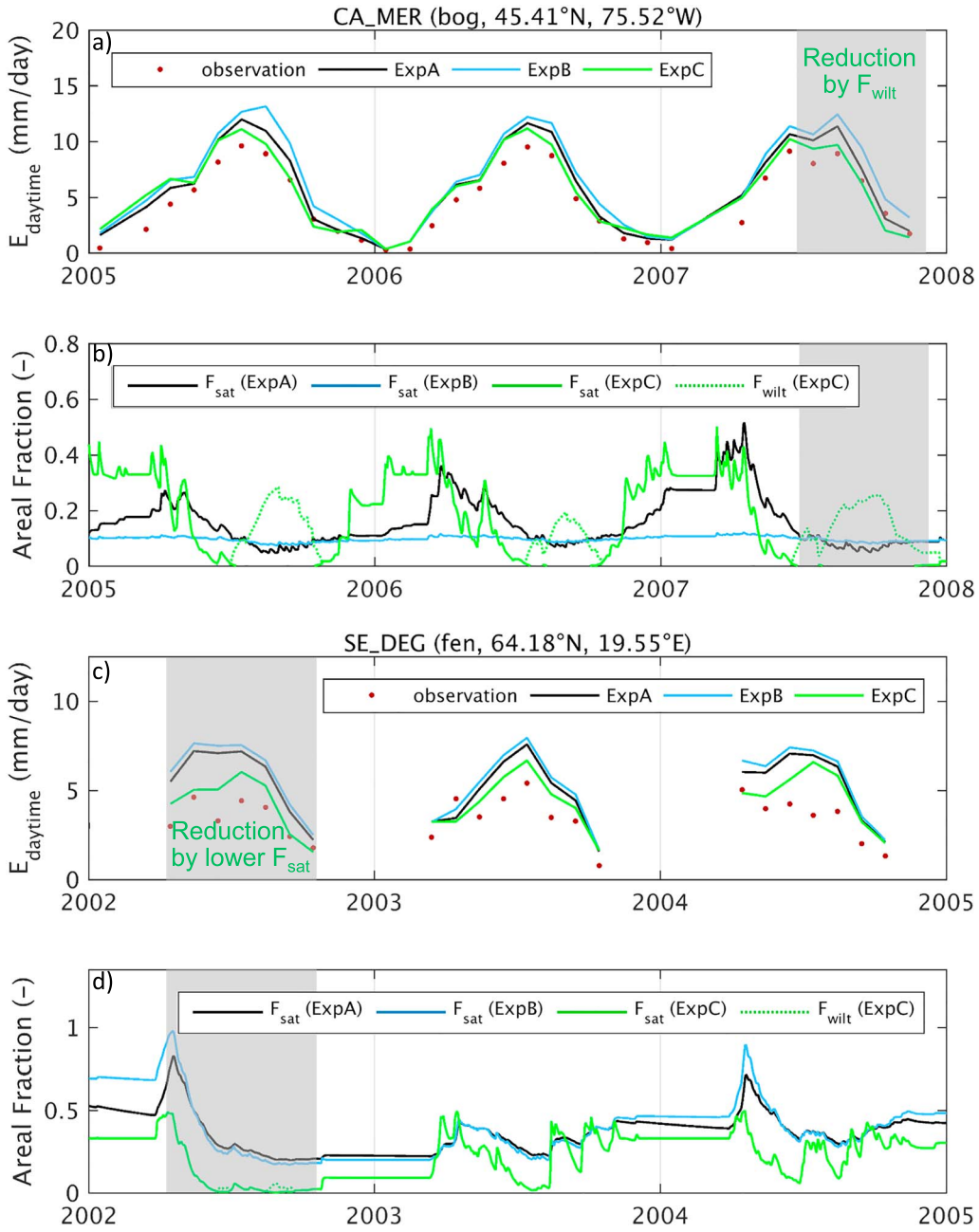

Figure B1. Monthly averaged daytime evapotranspiration ($E_{daytime}$) at (a) Mer Bleue (CA_MER) and (c) Degerö (SE_DEG). Shown are (red dots) field observations and results from the 30″ simulations of (black) ExpA, (blue) ExpB, and (green) ExpC. The corresponding daily time series of simulated areal fractions of saturated (F_{sat}) and wilting (F_{wilt}) regimes are shown in (b) and (d). ExpC was the only model that simulated values of F_{wilt} greater than zero. Periods with a gray background are further discussed in the text.

Magnus Lund, Maria Strack, Region Hannover, Global Institute for Water Security (University of Saskatchewan), Finnish Meteorological Institute, Oak Ridge National Laboratory, Mukhrino field station, Biebrza National Park, and Sun Gro Horticulture Canada.

Burdun, I., Sagris, V., & Mander, Ü. (2019). Relationships between field-measured hydrometeorological variables and satellite-based land surface temperature in a hemiboreal raised bog. *International Journal of Applied Earth Observation and Geoinformation*, *74*, 295–301. https://doi.org/https://doi.org/10.1016/j.jag.2018.09.019

Camacho, F., Cernicharo, J., Lacaze, R., Baret, F., & Weiss, M. (2013). GEOV1: LAI, FAPAR essential climate variables and FCOVER global time series capitalizing over existing products. Part 2: Validation and intercomparison with reference products. *Remote Sensing of Environment*, *137*, 310–329. https://doi.org/10.1016/j.rse.2013.02.030

Campbell, G. S. (1974). A simple method for determining unsaturated conductivity from moisture retention data. *Soil Science*, *117*(6), 311–314. https://doi.org/10.1097/00010694-197406000-00001

Chadburn, S. E., Burke, E. J., Essery, R. L. H., Boike, J., Langer, M., Heikenfeld, M., et al. (2015). Impact of model developments on present and future simulations of permafrost in a global land-surface model. *Cryosphere*, *9*(4), 1505–1521. https://doi.org/10.5194/tc-9-1505-2015

Clapp, R. B., & Hornberger, G. M. (1978). Empirical equations for some soil hydraulic properties. *Water Resources Research*, *14*(4), 601–604. https://doi.org/10.1029/WR014i004p00601

Clymo, R. S., Turunen, J., & Tolonen, K. (1998). Carbon accumulation in peatland. *Oikos*, *81*(2), 368. https://doi.org/10.2307/3547057

Cosby, B. J., Hornberger, G. M., Clapp, R. B., & Ginn, T. R. (1984). A statistical exploration of the relationships of soil moisture characteristics to the physical properties of soils. *Water Resources Research*, *20*(6), 682–690. https://doi.org/10.1029/WR020i006p00682

De Lannoy, G. J. M., Koster, R. D., Reichle, R. H., Mahanama, S. P. P., & Liu, Q. (2014). An updated treatment of soil texture and associated hydraulic properties in a global land modeling system. *Journal of Advances in Modeling Earth Systems*, *6*, 957–979. https://doi.org/10.1002/2014MS000330

De Lannoy, G. J. M., & Reichle, R. H. (2016). Global assimilation of multiangle and multipolarization SMOS brightness temperature observations into the GEOS-5 Catchment Land Surface Model for soil moisture estimation. *Journal of Hydrometeorology*, *17*(2), 669–691. https://doi.org/10.1175/JHM-D-15-0037.1

Dettmann, U., & Bechtold, M. (2016a). Deriving effective soil water retention characteristics from shallow water table fluctuations in peatlands. *Vadose Zone Journal*, *15*(10). https://doi.org/10.2136/vzj2016.04.0029

Dettmann, U., & Bechtold, M. (2016b). One-dimensional expression to calculate specific yield for shallow groundwater systems with microrelief. *Hydrological Processes*, *30*(2), 334–340. https://doi.org/10.1002/hyp.10637

Dettmann, U., Bechtold, M., Frahm, E., & Tiemeyer, B. (2014). On the applicability of unimodal and bimodal van Genuchten-Mualem based models to peat and other organic soils under evaporation conditions. *Journal of Hydrology*, *515*, 103–115. https://doi.org/10.1016/j.jhydrol.2014.04.047

Devito, K. J., Creed, I. F., & Fraser, C. J. D. (2005). Controls on runoff from a partially harvested aspen-forested headwater catchment, Boreal Plain, Canada. *Hydrological Processes*, *19*(1), 3–25. https://doi.org/10.1002/hyp.5776

Devito, K. J., Hokanson, K. J., Moore, P. A., Kettridge, N., Anderson, A. E., Chasmer, L., et al. (2017). Landscape controls on long-term runoff in subhumid heterogeneous Boreal Plains catchments. *Hydrological Processes*, *31*(15), 2737–2751. https://doi.org/10.1002/hyp.11213

Devito, K. J., Mendoza, C., & Qualizza, C. (2012). Conceptualizing water movement in the Boreal Plains: Implications for watershed reconstruction. Synthesis report prepared for the Canadian Oil Sands Network for Research and Development, Environmental and Reclamation Research Group. 164 pp.

Dimitrov, D. D., Grant, R. F., Lafleur, P. M., & Humphreys, E. R. (2010). Modeling the subsurface hydrology of Mer Bleue Bog. *Soil Science Society of America Journal*, *74*(2). https://doi.org/10.2136/sssaj2009.0148

Dimitrov, D. D., Grant, R. F., Lafleur, P. M., & Humphreys, E. R. (2011). Modeling the effects of hydrology on gross primary productivity and net ecosystem productivity at Mer Bleue bog. *Journal of Geophysical Research*, *116*, G04010. https://doi.org/10.1029/2010JG001586

Dinsmore, K. J., Drewer, J., Levy, P. E., George, C., Lohila, A., Aurela, M., & Skiba, U. M. (2017). Growing season CH_4 and N_2O fluxes from a subarctic landscape in northern Finland: From chamber to landscape scale. *Biogeosciences*, *14*(4), 799–815. https://doi.org/10.5194/bg-14-799-2017

Dirmeyer, P., & Oki, T. (2002). The Second Global Soil Wetness Project (GSWP-2) Science and Implementation Plan. IGPO Publication Series No. 37.

Dixon, S. J., Kettridge, N., Moore, P. A., Devito, K. J., Tilak, A. S., Petrone, R. M., et al. (2017). Peat depth as a control on moss water availability under evaporative stress. *Hydrological Processes*, *31*(23), 4107–4121. https://doi.org/10.1002/hyp.11307

Dorrepaal, E., Toet, S., van Logtestijn, R. S. P., Swart, E., van de Weg, M. J., Callaghan, T. V., & Aerts, R. (2009). Carbon respiration from subsurface peat accelerated by climate warming in the subarctic. *Nature*, *460*(7255), 616–619. https://doi.org/10.1038/nature08216

Du, J., Kimball, J. S., Galantowicz, J., Kim, S. B., Chan, S. K., Reichle, R., et al. (2018). Assessing global surface water inundation dynamics using combined satellite information from SMAP, AMSR2 and Landsat. *Remote Sensing of Environment*, *213*, 1–17. https://doi.org/10.1016/j.rse.2018.04.054

Ducharne, A., Koster, R. D., Suarez, M. J., Stieglitz, M., & Kumar, P. (2000). A catchment-based approach to modeling land surface processes in a general circulation model: 2. Parameter estimation and model demonstration. *Journal of Geophysical Research*, *105*(D20), 24,823–24,838. https://doi.org/10.1029/2000JD900328

Elmes, M. C., Thompson, D. K., Sherwood, J. H., & Price, J. S. (2018). Hydrometeorological conditions preceding wildfire, and the subsequent burning of a fen watershed in Fort McMurray, Alberta, Canada. *Natural Hazards and Earth System Sciences*, *18*(1), 157–170. https://doi.org/10.5194/nhess-18-157-2018

Eppinga, M. B., Rietkerk, M., Borren, W., Lapshina, E. D., Bleuten, W., & Wassen, M. J. (2008). Regular surface patterning of peatlands: Confronting theory with field data. *Ecosystems*, *11*(4), 520–536. https://doi.org/10.1007/s10021-008-9138-z

Fitzgerald, D. F., Price, J. S., & Gibson, J. J. (2003). Hillslope-swamp interactions and flow pathways in a hypermaritime rainforest, British Columbia. *Hydrological Processes*, *17*(15), 3005–3022. https://doi.org/10.1002/hyp.1279

Flanagan, L. B., & Syed, K. H. (2011). Stimulation of both photosynthesis and respiration in response to warmer and drier conditions in a boreal peatland ecosystem. *Global Change Biology*, *17*(7), 2271–2287. https://doi.org/10.1111/j.1365-2486.2010.02378.x

FLUXNET CANADA TEAM (2016). FLUXNET Canada Research Network—Canadian Carbon Program Data Collection, 1993-2014. Retrieved from https://doi.org/10.3334/ORNLDAAC/1335

Frank, S., Tiemeyer, B., Gelbrecht, J., & Freibauer, A. (2014). High soil solution carbon and nitrogen concentrations in a drained Atlantic bog are reduced to natural levels by 10 years of rewetting. *Biogeosciences*, *11*(8), 2309–2324. https://doi.org/10.5194/bg-11-2309-2014

Frei, S., Lischeid, G., & Fleckenstein, J. H. (2010). Effects of micro-topography on surface–subsurface exchange and runoff generation in a virtual riparian wetland — A modeling study. *Advances in Water Resources*, *33*(11), 1388–1401. https://doi.org/10.1016/j.advwatres.2010.07.006

Frolking, S., & Roulet, N. T. (2007). Holocene radiative forcing impact of northern peatland carbon accumulation and methane emissions. *Global Change Biology*, *13*(5), 1079–1088. https://doi.org/10.1111/j.1365-2486.2007.01339.x

Frolking, S., Roulet, N. T., Moore, T. R., Lafleur, P. M., Bubier, J. L., & Crill, P. M. (2002). Modeling seasonal to annual carbon balance of Mer Bleue Bog, Ontario, Canada. *Global Biogeochemical Cycles.*, *16*(3), 1030. https://doi.org/10.1029/2001GB001457

Frolking, S., Roulet, N. T., Tuittila, E., Bubier, J. L., Quillet, A., Talbot, J., & Richard, P. J. H. (2010). A new model of Holocene peatland net primary production, decomposition, water balance, and peat accumulation. *Earth System Dynamics Discussions*, *1*(1), 115–167. https://doi.org/10.5194/esdd-1-115-2010

Frolking, S., Talbot, J., Jones, M. C., Treat, C. C., Kauffman, J. B., Tuittila, E.-S., & Roulet, N. (2011). Peatlands in the Earth's 21st century climate system. *Environmental Reviews*, *19*(NA), 371–396. https://doi.org/10.1139/a11-014

Gelaro, R., McCarty, W., Suárez, M. J., Todling, R., Molod, A., Takacs, L., et al. (2017). The Modern-Era Retrospective Analysis for Research and Applications, version 2 (MERRA-2). *Journal of Climate*, *30*(14), 5419–5454. https://doi.org/10.1175/JCLI-D-16-0758.1

Gong, J., Wang, K., Kellomäki, S., Zhang, C., Martikainen, P. J., & Shurpali, N. (2012). Modeling water table changes in boreal peatlands of Finland under changing climate conditions. *Ecological Modelling*, *244*, 65–78. https://doi.org/10.1016/j.ecolmodel.2012.06.031

Granberg, G., Grip, H., Ottosson Löfvenius, M., Sundh, I., Svensson, B. H., & Nilsson, M. (1999). A simple model for simulation of water content, soil frost, and soil temperatures in boreal mixed mires. *Water Resources Research*, *35*(12), 3771–3782. https://doi.org/10.1029/1999WR900216

Grant, R. F., Desai, A. R., & Sulman, B. N. (2012). Modelling contrasting responses of wetland productivity to changes in water table depth. *Biogeosciences*, *9*(11), 4215–4231. https://doi.org/10.5194/bg-9-4215-2012

Grygoruk, M., Batelaan, O., Okruszko, T., Mirosław-Świątek, D., Chormański, J., & Rycharski, M. (2011). Groundwater modelling and hydrological system analysis of wetlands in the Middle Biebrza Basin. In T. Okruszko, & D. Mirosław-Świątek (Eds.), *Hydrological Processes in the Narew Catchment*, (pp. 89–109). Springer. https://doi.org/https://doi.org/10.1007/978-3-642-19059-9_6

Hanson, P. J., Riggs, J. S., Dorrance, C., Nettles, W. R., & Hook, L. A. (2015). SPRUCE Environmental Monitoring Data: 2010-2016. Retrieved from https://doi.org/10.3334/CDIAC/spruce.001

Hogan, J. M., van der Kamp, G., Barbour, S. L., & Schmidt, R. (2006). Field methods for measuring hydraulic properties of peat deposits. *Hydrological Processes*, *20*(17), 3635–3649. https://doi.org/10.1002/hyp.6379

Hokanson, K. J., Lukenbach, M. C., Devito, K. J., Kettridge, N., Petrone, R. M., & Waddington, J. M. (2016). Groundwater connectivity controls peat burn severity in the boreal plains. *Ecohydrology*, *9*(4), 574–584. https://doi.org/10.1002/eco.1657

Hokanson, K. J., Mendoza, C. A., & Devito, K. J. (2019). Interactions Between Regional Climate, Surficial Geology, and Topography: Characterizing Shallow Groundwater Systems in Subhumid, Low-Relief Landscapes. *Water Resources Research*, *55*, 284–297. https://doi.org/10.1029/2018WR023934

Holden, J., & Burt, T. P. (2003). Runoff production in blanket peat covered catchments. *Water Resources Research*, *39*(7), 1191. https://doi.org/10.1029/2002WR001956

Hommeltenberg, J., Mauder, M., Drösler, M., Heidbach, K., Werle, P., & Schmid, H. P. (2014). Ecosystem scale methane fluxes in a natural temperate bog-pine forest in southern Germany. *Agricultural and Forest Meteorology*, *198-199*, 273–284. https://doi.org/10.1016/j.agrformet.2014.08.017

Hooijer, A., Page, S., Canadell, J. G., Silvius, M., Kwadijk, J., Wösten, H., & Jauhiainen, J. (2010). Current and future CO_2 emissions from drained peatlands in Southeast Asia. *Biogeosciences*, *7*(5), 1505–1514. https://doi.org/10.5194/bg-7-1505-2010

Humphreys, E. R., Lafleur, P. M., Flanagan, L. B., Hedstrom, N., Syed, K. H., Glenn, A. J., & Granger, R. (2006). Summer carbon dioxide and water vapor fluxes across a range of northern peatlands. *Journal of Geophysical Research*, *111*, G04011. https://doi.org/10.1029/2005JG000111

Hurkuck, M., Brümmer, C., Mohr, K., Grünhage, L., Flessa, H., & Kutsch, W. L. (2014). Determination of atmospheric nitrogen deposition to a semi-natural peat bog site in an intensively managed agricultural landscape. *Atmospheric Environment*, *97*, 296–309. https://doi.org/10.1016/j.atmosenv.2014.08.034

Ingram, H. A. P. (1978). Soil layers in mires: Function and terminology. *Journal of Soil Science*, *29*(2), 224–227. https://doi.org/10.1111/j.1365-2389.1978.tb02053.x

Intergovernmental Panel on Climate Change (2014). Climate Change 2013—The Physical Science Basis. Climate Change 2013 - The Physical Science Basis, Contribution to the Fifth Assessment Report of the Intergovernmental Panel on Climate Change. https://doi.org/10.1017/CBO9781107415324

Ivanov, K. E. (1981). *Water movement in Mirelands. Academic Press*. London: Academic Press.

Johnson, L. C., Damman, A. W. H., & Malmer, N. (1990). Sphagnum Macrostructure as an Indicator of Decay and Compaction in Peat Cores from an Ombrotrophic South Swedish Peat-Bog. *Journal of Ecology*, *78*(3), 633–647.

Joosten, H., & Clarke, D. (2002). Wise use of mires and peatlands—Background and principles including a framework for decision-making. International Mire Conservation Group and International Peat Society.

Kienzle, S. (2004). The effect of DEM raster resolution on first order, second order and compound terrain derivatives. *Transactions in GIS*, *8*(1), 83–111. https://doi.org/10.1111/j.1467-9671.2004.00169.x

Kettridge, N., Comas, X., Baird, A., Slater, L., Strack, M., Thompson, D., et al. (2008). Ecohydrologically important subsurface structures in peatlands revealed by ground-penetrating radar and complex conductivity surveys. *Journal of Geophysical Research*, *113*, G04030. https://doi.org/10.1029/2008jg000787

Koster, R. (2015). "Efficiency space": A framework for evaluating joint evaporation and runoff behavior. *Bulletin of the American Meteorological Society*, *96*(3), 393–396. https://doi.org/10.1175/BAMS-D-14-00056.1

Koster, R. D., & Suarez, M. J. (1991). A simplified treatment of SiB's land surface albedo parameterization. NASA Technical Memorandum 104538, Greenbelt, MD: Goddard Space Flight Center.

Koster, R. D., & Suarez, M. J. (1992). Modeling the land surface boundary in climate models as a composite of independent vegetation stands. *Journal of Geophysical Research*, *97*(D3), 2697–2715. https://doi.org/10.1029/91JD01696

Koster, R. D., Suarez, M. J., Ducharne, A., Stieglitz, M., & Kumar, P. (2000). A catchment-based approach to modeling land surface processes in a general circulation model: 1. Model structure. *Journal of Geophysical Research*, *105*(D20), 24809. https://doi.org/10.1029/2000JD900327

Koster, R. D., & Walker, G. K. (2015). Interactive vegetation phenology, soil moisture, and monthly temperature forecasts. *Journal of Hydrometeorology*, *16*(4), 1456–1465. https://doi.org/10.1175/JHM-D-14-0205.1

Kurbatova, J., Li, C., Tatarinov, F., Varlagin, A., Shalukhina, N., & Olchev, A. (2009). Modeling of the carbon dioxide fluxes in European Russia peat bogs. *Environmental Research Letters*, *4*(4). https://doi.org/10.1088/1748-9326/4/4/045022

Lafleur, P. M. (2008). Connecting atmosphere and wetland: Energy and water vapour exchange. *Geography Compass*, *2*(4), 1027–1057. https://doi.org/10.1111/j.1749-8198.2007.00132.x

Lafleur, P. M., Hember, R. A., Admiral, S. W., & Roulet, N. T. (2005). Annual and seasonal variability in evapotranspiration and water table at a shrub-covered bog in southern Ontario, Canada. *Hydrological Processes*, *19*(18), 3533–3550. https://doi.org/10.1002/hyp.5842

Lawrence, D. M., & Slater, A. G. (2008). Incorporating organic soil into a global climate model. *Climate Dynamics*, *30*(2–3), 145–160. https://doi.org/10.1007/s00382-007-0278-1

Letts, M. G., Comer, N. T., Roulet, N. T., Skarupa, M. R., & Verseghy, D. L. (2000). Parametrization of peatland hydraulic properties for the Canadian land surface scheme. *Atmosphere - Ocean*, *38*(1), 141–160. https://doi.org/10.1080/07055900.2000.9649643

Limpens, J., Berendse, F., Blodau, C., Canadell, J. G., Freeman, C., Holden, J., et al. (2008). Peatlands and the carbon cycle: From local processes to global implications—A synthesis. *Biogeosciences*, *5*(5), 1475–1491. https://doi.org/10.5194/bg-5-1475-2008

Loisel, J., Yu, Z., Beilman, D. W., Camill, P., Alm, J., Amesbury, M. J., et al. (2014). A database and synthesis of northern peatland soil properties and Holocene carbon and nitrogen accumulation. *Holocene*, *24*(9), 1028–1042. https://doi.org/10.1177/0959683614538073

Lukenbach, M. C., Hokanson, K. J., Devito, K. J., Kettridge, N., Petrone, R. M., Mendoza, C. A., et al. (2017). Post-fire ecohydrological conditions at peatland margins in different hydrogeological settings of the Boreal Plain. *Journal of Hydrology*, *548*, 741–753. https://doi.org/10.1016/j.jhydrol.2017.03.034

Lund, M., Christensen, T. R., Lindroth, A., & Schubert, P. (2012). Effects of drought conditions on the carbon dioxide dynamics in a temperate peatland. *Environmental Research Letters*, *7*(4). https://doi.org/10.1088/1748-9326/7/4/045704

Mahanama, S. P., Koster, R. D., Walker, G. K., Takacs, L. L., Reichle, R. H., De Lannoy, G. J. M., et al. (2015). Land boundary conditions for the Goddard Earth Observing System Model Version 5 (GEOS-5) Climate Modeling System: Recent updates and data file descriptions. Technical Report Series on Global Modeling and Data Assimilation, Volume 39. Greenbelt, MD*:* NASA Goddard Space Flight Center.

Malhotra, A., Roulet, N. T., Wilson, P., Giroux-Bougard, X., & Harris, L. I. (2016). Ecohydrological feedbacks in peatlands: An empirical test of the relationship among vegetation, microtopography and water table. *Ecohydrology*, *9*(7), 1346–1357. https://doi.org/10.1002/eco.1731

Mauder, M., Cuntz, M., Drüe, C., Graf, A., Rebmann, C., Schmid, H. P., et al. (2013). A strategy for quality and uncertainty assessment of long-term eddy-covariance measurements. *Agricultural and Forest Meteorology*, *169*, 122–135. https://doi.org/10.1016/j.agrformet.2012.09.006

McCarter, C. P. R., & Price, J. S. (2014). Ecohydrology of Sphagnum moss hummocks: Mechanisms of capitula water supply and simulated effects of evaporation. *Ecohydrology*, *7*(1), 33–44. https://doi.org/10.1002/eco.1313

Melton, J. R., Wania, R., Hodson, E. L., Poulter, B., Ringeval, B., Spahni, R., et al. (2013). Present state of global wetland extent and wetland methane modelling: Conclusions from a model inter-comparison project (WETCHIMP). *Biogeosciences*, *10*(2), 753–788. https://doi.org/10.5194/bg-10-753-2013

Metzger, C., Jansson, P.-E., Lohila, A., Aurela, M., Eickenscheidt, T., Belelli-Marchesini, L., et al. (2015). CO_2 fluxes and ecosystem dynamics at five European treeless peatlands—Merging data and process oriented modeling. *Biogeosciences*, *12*(1), 125–146. https://doi.org/10.5194/bg-12-125-2015

Millard, K., & Richardson, M. (2018). Quantifying the relative contributions of vegetation and soil moisture conditions to polarimetric C-Band SAR response in a temperate peatland. *Remote Sensing of Environment*, *206*, 123–138. https://doi.org/10.1016/j.rse.2017.12.011

Moody, E. G. (2008). MODIS-derived spatially complete surface albedo products: Spatial and temporal pixel and zonal averages. *Journal of Applied Meteorology and Climatology*, *47*(11), 2879–2894. https://doi.org/10.1175/2008JAMC1795.1

Morris, P. J., Baird, A. J., & Belyea, L. R. (2012). The DigiBog peatland development model 2: Ecohydrological simulations in 2D. *Ecohydrology*, *5*(3), 256–268. https://doi.org/10.1002/eco.229

Morris, P. J., Baird, A. J., & Belyea, L. R. (2015). Bridging the gap between models and measurements of peat hydraulic conductivity. *Water Resources Research*, *51*, 5353–5364. https://doi.org/10.1002/2015WR017264

Munir, T. M., Perkins, M., Kaing, E., & Strack, M. (2015). Carbon dioxide flux and net primary production of a boreal treed bog: Responses to warming and water-table-lowering simulations of climate change. *Biogeosciences*, *12*(4), 1091–1111. https://doi.org/10.5194/bg-12-1091-2015

Nijp, J. J., Metselaar, K., Limpens, J., Teutschbein, C., Peichl, M., Nilsson, M. B., et al. (2017). Including hydrological self-regulating processes in peatland models: Effects on peatmoss drought projections. *Science of the Total Environment*, *580*, 1389–1400. https://doi.org/10.1016/j.scitotenv.2016.12.104

Nungesser, M. K. (2003). Modelling microtopography in boreal peatlands: Hummocks and hollows. *Ecological Modelling*, *165*(2–3), 175–207. https://doi.org/10.1016/S0304-3800(03)00067-X

Peichl, M., Sagerfors, J., Lindroth, A., Buffam, I., Grelle, A., Klemedtsson, L., et al. (2013). Energy exchange and water budget partitioning in a boreal minerogenic mire. *Journal of Geophysical Research: Biogeosciences*, *118*, 1–13. https://doi.org/10.1029/2012JG002073

Price, J. S. (1996). Hydrology and microclimate of a partly restored cutover bog, Quebec. *Hydrological Processes*, *10*(10), 1263–1272. https://doi.org/10.1002/(SICI)1099-1085(199610)10:10<1263::AID-HYP458>3.0.CO;2-1

Price, J. (1997). Soil moisture, water tension, and water table relationships in a managed cutover bog. *Journal of Hydrology*, *202*(1–4), 21–32.

Qiu, C., Zhu, D., Ciais, P., Guenet, B., Krinner, G., Peng, S., et al. (2018). ORCHIDEE-PEAT (revision 4596), a model for northern peatland CO_2, water, and energy fluxes on daily to annual scales. *Geoscientific Model Development*, *11*(2), 497–519. https://doi.org/10.5194/gmd-11-497-2018

Reichle, R., Draper, C., Liu, Q., Girotto, M., Mahanama, S., Koster, R., & De Lannoy, G. J. M. (2017). Assessment of MERRA-2 land surface hydrology estimates. *Journal of Climate*, *18*(7), 861–878. https://doi.org/10.1080/09669581003782739

Reichle, R. H., de Lannoy, G. J. M., Liu, Q., Koster, R. D., Kimball, J. S., Crow, W. T., et al. (2017). Global assessment of the SMAP Level-4 surface and root-zone soil moisture product using assimilation diagnostics. *Journal of Hydrometeorology*, *18*(12), 3217–3237. https://doi.org/10.1175/JHM-D-17-0130.1

Reichle, R. H., Liu, Q., Koster, R. D., Ardizzone, J. V., Colliander, A., Crow, W. T., et al. (2018). Soil Moisture Active Passive (SMAP) project assessment report for version 4 of the L4_SM data product. Technical Report Series on Global Modeling and Data Assimilation, Volume 52*,* MD*:* NASA Goddard Space Flight Center.

Reichle, R. H., Liu, Q., Koster, R. D., Draper, C. S., Mahanama, S. P. P., & Partyka, G. S. (2017). Land surface precipitation in MERRA-2. *Journal of Climate*, *30*(5), 1643–1664. https://doi.org/10.1175/JCLI-D-16-0570.1

Reynolds, C. A., Jackson, T. J., & Rawls, W. J. (2000). Estimating soil water-holding capacities by linking the Food and Agriculture Organization soil map of the world with global pedon databases and continuous pedotransfer functions. *Water Resources Research*, *36*(12), 3653–3662. https://doi.org/10.1029/2000WR900130

Rezanezhad, F., Price, J. S., & Craig, J. R. (2012). The effects of dual porosity on transport and retardation in peat: A laboratory experiment. *Canadian Journal of Soil Science*, *92*(5), 723–732. https://doi.org/10.4141/cjss2011-050

Rochefort, L., Vitt, D. H., & Bayley, S. E. (1990). Growth, Production, and Decomposition Dynamics of Sphagnum under Natural and Experimentally Acidified Conditions. *Ecology*, *71*(5, 1986–2000.

Romanov, V. V. (1968). Hydrophysics of bogs. Jerusalem: Israel Program of Scientific Translations.

Rydin, H., Gunnarsson, U., & Sundberg, S. (2006). The role of Sphagnum in peatland development and persistence. In R. K. Wieder & D. H. Vitt (Eds.), *Boreal Peatland Ecosystems*, (Vol. 188, pp. 47–65). Springer, Ecological Studies. https://doi.org/10.1007/978-3-540-31913-9_4

Schouwenaars, J. M. (1990). Problem-oriented studies on plant-soil-water relations. PhD-thesis, Wageningen Agricultural University.

Sellers, P. J., Mintz, Y., Sud, Y. C., & Dalcher, A. (1986). A simple biosphere model (SIB) for use within general circulation models. *Journal of the Atmospheric Sciences*, *43*(6), 505–531. https://doi.org/10.1175/1520-0469(1986)043<0505:ASBMFU>2.0.CO;2

Shi, X., Thornton, P. E., Ricciuto, D. M., Hanson, P. J., Mao, J., Sebestyen, S. D., et al. (2015). Representing northern peatland microtopography and hydrology within the Community Land Model. *Biogeosciences*, *12*(21), 6463–6477. https://doi.org/10.5194/bg-12-6463-2015

Sonnentag, O., Chen, J. M., Roulet, N. T., Ju, W., & Govind, A. (2008). Spatially explicit simulation of peatland hydrology and carbon dioxide exchage: Influence of mesoscale topography. *Journal of Geophysical Research*, *113*, G02005. https://doi.org/10.1029/2007JG000605

Sonnentag, O., van der Kamp, G., Barr, A. G., & Chen, J. M. (2010). On the relationship between water table depth and water vapor and carbon dioxide fluxes in a minerotrophic fen. *Global Change Biology*, *16*(6), 1762–1776. https://doi.org/10.1111/j.1365-2486.2009.02032.x

St-Hilaire, F., Wu, J., Roulet, N. T., Frolking, S., Lafleur, P. M., Humphreys, E. R., & Arora, V. (2010). McGill wetland model: Evaluation of a peatland carbon simulator developed for global assessments. *Biogeosciences*, *7*(11), 3517–3530. https://doi.org/10.5194/bg-7-3517-2010

Stieglitz, M., Ducharne, A., Koster, R., & Suarez, M. (2001). The impact of detailed snow physics on the simulation of snow cover and subsurface thermodynamics at continental scales. *Journal of Hydrometeorology*, *2*(3), 228–242. https://doi.org/10.1175/1525-7541(2001)002<0228:TIODSP>2.0.CO;2

Stoy, P. C., Mauder, M., Foken, T., Marcolla, B., Boegh, E., Ibrom, A., et al. (2013). A data-driven analysis of energy balance closure across FLUXNET research sites: The role of landscape scale heterogeneity. *Agricultural and Forest Meteorology*, *171-172*, 137–152. https://doi.org/10.1016/j.agrformet.2012.11.004

Strack, M., Waddington, J. M., Rochefort, L., & Tuittila, E. S. (2006). Response of vegetation and net ecosystem carbon dioxide exchange at different peatland microforms following water table drawdown. *Journal of Geophysical Research*, *111*, G02006. https://doi.org/10.1029/2005JG000145

Sulman, B. N., Desai, A. R., Cook, B. D., Saliendra, N., & MacKay, D. S. (2009). Contrasting carbon dioxide fluxes between a drying shrub wetland in Northern Wisconsin, USA, and nearby forests. *Biogeosciences*, *6*(6), 1115–1126. https://doi.org/10.5194/bg-6-1115-2009

Tao, J., Reichle, R. H., Koster, R. D., Forman, B. A., & Xue, Y. (2017). Evaluation and enhancement of permafrost modeling with the NASA Catchment Land Surface Model. *Journal of Advances in Modeling Earth Systems*, *9*, 2771–2795. https://doi.org/10.1002/2017MS001019

Terentieva, I. E., Glagolev, M. V., Lapshina, E. D., Sabrekov, A. F., & Maksyutov, S. (2016). Mapping of West Siberian taiga wetland complexes using Landsat imagery: Implications for methane emissions. *Biogeosciences*, *13*(16), 4615–4626. https://doi.org/10.5194/bg-13-4615-2016

Tubiello, F. N., Biancalani, R., Salvatore, M., Rossi, S., & Conchedda, G. (2016). A worldwide assessment of greenhouse gas emissions from drained organic soils. *Sustainability*, *8*(4). https://doi.org/10.3390/su8040371

van der Schaaf, S. (1999). Analysis of the hydrology of raised bogs in the Irish Midlands—A case study of Ranheenmore Bog and Clara Bog. PhD-thesis, Wageningen Agricultural University.

Virta, J. (1966). Measurement of evapotranspiration and computation of water budget in treeless peatlands in the natural state. Commentationes Physico-Mathematicae. *Social Science Fennici*, *32*(11), 1–70.

Waddington, J. M., Morris, P. J., Kettridge, N., Granath, G., Thompson, D. K., & Moore, P. A. (2015). Hydrological feedbacks in northern peatlands. *Ecohydrology*, *8*(1), 113–127. https://doi.org/10.1002/eco.1493

Wania, R., Ross, L., & Prentice, I. C. (2009). Integrating peatlands and permafrost into a dynamic global vegetation model: 1. Evaluation and sensitivity of physical land surface processes. *Global Biogeochemical Cycles*, *23*, GB3014. https://doi.org/10.1029/2008GB003412

Weber, T. K. D., Iden, S. C., & Durner, W. (2017). Unsaturated hydraulic properties of Sphagnum moss and peat reveal trimodal pore-size distributions. *Water Resources Research*, *53*, 415–434. https://doi.org/10.1002/2016WR019707

Weiss, R., Shurpali, N. J., Sallantaus, T., Laiho, R., Laine, J., & Alm, J. (2006). Simulation of water table level and peat temperatures in boreal peatlands. *Ecological Modelling*, *192*(3–4), 441–456. https://doi.org/10.1016/j.ecolmodel.2005.07.016

Wells, C., Ketcheson, S., & Price, J. (2017). Hydrology of a wetland-dominated headwater basin in the Boreal Plain, Alberta, Canada. *Journal of Hydrology*, *547*, 168–183. https://doi.org/10.1016/j.jhydrol.2017.01.052

Wells, C. M., & Price, J. S. (2015). A hydrologic assessment of a saline-spring fen in the Athabasca oil sands region, Alberta, Canada—A potential analogue for oil sands reclamation. *Hydrological Processes*, *29*(20), 4533–4548. https://doi.org/10.1002/hyp.10518

Whittington, P. N., & Price, J. S. (2006). The effects of water table draw-down (as a surrogate for climate change) on the hydrology of a fen peatland, Canada. *Hydrological Processes*, *20*(17), 3589–3600. https://doi.org/10.1002/hyp.6376

Wösten, J. H. M., Veerman, G. ., DeGroot, W. J. ., & Stolte, J. (2001). Waterretentie- en doorlatendheidskarakteristieken van boven- en ondergronden in Nederland: De Staringreeks. vernieuwde uitgave 2001, Alterra Rapp. 153, Alterra, Res. Inst. voor de Groene Ruimte, Wageningen, Netherlands.

Wu, Y., & Blodau, C. (2013). PEATBOG: A biogeochemical model for analyzing coupled carbon and nitrogen dynamics in northern peatlands. *Geoscientific Model Development*, *6*(4), 1173–1207. https://doi.org/10.5194/gmd-6-1173-2013

Wu, Y., Verseghy, D. L., & Melton, J. R. (2016). Integrating peatlands into the coupled Canadian Land Surface Scheme (CLASS) v3.6 and the Canadian Terrestrial Ecosystem Model (CTEM) v2.0. *Geoscientific Model Development*, *9*(8), 2639–2663. https://doi.org/10.5194/gmd-9-2639-2016

Xu, J., Morris, P. J., Liu, J., & Holden, J. (2018). PEATMAP: Refining estimates of global peatland distribution based on a meta-analysis. *Catena*, *160*, 134–140. https://doi.org/10.1016/j.catena.2017.09.010

Zhang, Y., Li, C., Trettin, C. C., Li, H., & Sun, G. (2002). An integrated model of soil, hydrology, and vegetation for carbon dynamics in wetland ecosystems. *Global Biogeochemical Cycles*, *16*(4), 1061. https://doi.org/10.1029/2001GB001838